SEISMIC BEHAVIOR OF VERTICAL REINFORCED AUTOCLAVED AERATED CONCRETE (AAC) PANEL WALLS

A THESIS SUBMITTED TO
THE GRADUATE SCHOOL OF NATURAL AND APPLIED SCIENCES
OF
MIDDLE EAST TECHNICAL UNIVERSITY

ARMIN TAGHIPOUR

IN PARTIAL FULFILLMENT OF THE REQUIREMENTS
FOR
THE DEGREE OF MASTER OF SCIENCE
IN
CIVIL ENGINEERING

SEPTEMBER 2016

Approval of the thesis:

SEISMIC BEHAVIOR OF VERTICAL REINFORCED AUTOCLAVED AERATED CONCRETE (AAC) PANEL WALLS

submitted by **ARMIN TAGHIPOUR** in partial fulfillment of the requirements for the degree of **Master of Science in Civil Engineering Department, Middle East Technical University** by,

Prof. Dr. Gülbin Dural Ünver _____
Dean, Graduate School of **Natural and Applied Sciences**

Prof. Dr. İsmail Özgür Yaman _____
Head of Department, **Civil Engineering**

Prof. Dr. Erdem Canbay _____
Supervisor, **Civil Engineering Department, METU**

Prof. Dr. Barış Binici _____
Co-supervisor, **Civil Engineering Department, METU**

Examining Committee Members:

Prof. Dr. Ahmet Yakut
Civil Engineering Department, METU _____

Prof. Dr. Erdem Canbay
Civil Engineering Department, METU _____

Prof. Dr. Barış Binici
Civil Engineering Department, METU _____

Prof. Dr. Murat Altuğ Erberik
Civil Engineering Department, METU _____

Assoc. Prof. Dr. Sabahattin Aykaç
Civil Engineering Department, Gazi University _____

Date: 02.09.2016

I hereby declare that all information in this document has been obtained and presented in accordance with academic rules and ethical conduct. I also declare that, as required by these rules and conduct, I have fully cited and referenced all material and results that are not original to this work.

Name, Last Name: ARMIN TAGHIPOUR

Signature :

ABSTRACT

SEISMIC BEHAVIOR OF VERTICAL REINFORCED AUTOCLAVED AERATED CONCRETE (AAC) PANEL WALLS

Taghipour, Armin
M.S., Department of Civil Engineering
Supervisor : Prof. Dr. Erdem Canbay
Co-Supervisor : Prof. Dr. Barış Binici

September 2016, 90 pages

In this study, the in-plane seismic behavior of autoclaved aerated concrete (AAC) vertical load-bearing wall panels is examined. Because of the complex behavior of AAC shear walls under cyclic lateral loading and axial load, the design provisions are fundamentally important. The main objective of this study is to validate proposed design provisions for AAC structures in Turkey.

Six specimens with different properties and geometries were constructed and tested at Structural Mechanics Laboratory of METU. Mechanical properties of AAC were also determined at METU and were verified with test results at other laboratories.

AAC vertical wall panels were produced at AKG-Gazbeton. Test samples were made of various numbers of wall panel units, laid vertically. Specimens with two and four vertical units were tested with and without axial load. Finally, the samples with six vertical wall panels were tested with and without window

opening in specimen.

The tests were conducted by applying cyclic lateral load. Different measuring devices like LVDTs and Load Cells were installed to acquire the data and perceive the behavior of the samples. To verify the experimental results, an analytical model for each specimen was developed to compare the experimental and analytical results.

The value 3 for structural behavior factor, R, given in the new proposed Turkish Earthquake Code (TEC 2016) seems to be fairly acceptable and on the safe side according to the test results. Ultimate drift ratio should be limited to 1%. Both MSJC 2011 and draft TEC 2016 estimated many test results unsafely.

Keywords: Aerated Autoclaved Concrete, AAC, Vertical reinforced panel, Shear wall, Masonry structures, Experimental method.

ÖZ

DÜŞEY DONATILI GAZBETON PANEL DUVARLARIN SİSMİK DAVRANIŞI

Taghipour, Armin
Yüksek Lisans, İnşaat Mühendisliği Bölümü
Tez Yöneticisi : Prof. Dr. Erdem Canbay
Ortak Tez Yöneticisi : Prof. Dr. Barış Binici

Eylül 2016 , 90 sayfa

Bu çalışmada yük taşıyan düşey duvar Gazbeton panellerin düzlem içi sismik davranışı incelenmektedir. Gazbeton perde duvarların çevrimsel yatay yük ve düşey yük altındaki davranışı karmaşık olduğundan tasarım koşulları esasen çok önemlidir. Bu çalışmanın ana amacı Türkiye'deki Gazbeton yapılar için önerilen tasarım koşullarının doğrulanmasıdır.

Değişik özelliklerde ve geometride altı elaman ODTÜ Yapı Mekaniği Laboratuvarında inşa edilerek denenmiştir. Ayrıca Gazbetonun mekanik özellikleri belirlenmiş ve diğer laboratuvar deney sonuçlarıyla doğrulanmıştır. Gazbeton düşey paneller AKG-Gazbeton tarafından üretilmiştir. Deney elemanları değişik sayıdaki düşey panel birimlerinden oluşmaktadır. İki ve dört düşey panelli elamanlar eksenel yüklü ve eksenel yüksüz olarak test edilmiştir. Altı düşey panelli elamanlar ise pencere boşluklu ve boşluksuz olarak denenmişlerdir.

Deneyler çevrimsel yatay yükler altında gerçekleştirilmiştir. Veri toplayıp eleman davranışını algılamak için LVDT ve yük hücresi gibi farklı ölçüm cihazları kullanılmıştır. Deney sonuçlarını doğrulamak amacıyla her eleman için analitik model geliştirilmiştir.

Yeni önerilen Türk Deprem Yönetmeliğinde (TEC 2016) yapısal davranış katsayısı, R için verilen 3 değeri deney sonuçlarına göre oldukça kabul edilebilir ve güvenli durmaktadır. Maksimum öteleme oranı %1 ile sınırlandırılmalıdır. Hem MSJC 2011 hem de taslak TEC 2016 bir çok deney sonucuna güvensiz tarafta kestirmektedir.

Anahtar Kelimeler: Gazbeton, Düşey donatılı panel, Duvar, Sismik davranış, Yığma yapılar, Deneysel.

Dedicated with love and thanks to my family, who have given me so much along the way.

ACKNOWLEDGMENTS

I would like to express my sincere gratitude to my supervisor Prof. Dr. Erdem Canbay, and my co-supervisor Prof. Dr. Barış Binici for their continuous guidance, support, motivation and the confidence they have shown in me throughout my studies. Their constant encouragements in my dissertation work have helped me to look forward to the future with enthusiasm and confidence.

I owe my deepest and warmest thanks to my family who give me strength and encouragement throughout my studies. I am so grateful to my dad Mahmoud, my mom Hamideh and my brothers Kaveh and Farzam, for their everlasting supports both emotionally and financially, in completing this endeavor. They deserve my deepest gratitude for everything.

I would like to acknowledge the invaluable assistance of Alper Aldemir, who was always available for discussions on my dissertation ideas. I also appreciate the support of my friends Rasul Tarvirdilu Asl, Reza Zeinali, Milad Bybordiani, Ali Gharibdoust, Ramin Rouzbar, Payam Allahverdizadeh, Sadra Azizi, Siamak Pourkeivannour, and Vahid Haseltalab for always promoting me and believing in me throughout my studies.

Technical assistance provided by the METU Structural Engineering Laboratory staff is greatly acknowledged.

Finally, a special thanks goes out to my dearest friend, Nina Razi. Your support and praise was much appreciated and kept me going. In a sentence, the completion of this work would not have been possible without your help.

TABLE OF CONTENTS

LIST OF TABLES

TABLES

LIST OF FIGURES

FIGURES

CHAPTER 1

INTRODUCTION

1.1 General

The significant mechanical properties such as, the low specific weight, superior insulation properties, and easy installation makes the Autoclaved Aerated Concrete (AAC) one of the most important construction materials in the world. The use of lighter and lower density AAC is becoming more and more appealing because of its advantages such as, fire proof, insulation, fast construction, and light weight nature.

In recent years, AAC has been used in different types of constructions like residential, public facilities, schools, college dorms, and partition walls in different countries all over the world[1]. For instance, in 2008 during the International Builders' Show (IBS), The New American Home focused on sustainable construction and highlighted the advantages of AAC by constructing some model houses in Florida and Orlando. In Figure 1.1, a dormitory constructed at The New College of Florida is shown as one of the good applications of AAC panels [Wilson and Palmer, 2008]. Furthermore, in 1970's in China because of advantages of AAC panels, like great insulation, factory-made and assembly construction, AAC panels has been preferred to other materials in housing industry and has been used as exterior walls in buildings or industrial plants [Duan et al., 2014]. Moreover, in some of the European countries 60% of new building constructions uses different types of AAC panels or blocks. In the Middle

[1] AERCON AAC, `http://www.aerconaac.com/technical-manual-introduction.html#Applications`, last visited on August 2016

East, Australia and Far East, AAC is also as adequate material in constructions [Witfmann and Pytlik, 1992].

Aforementioned examples clearly shows that AAC construction can be a good alternative to masonry constructions. Hence, to guarantee the seismic and structural performance of buildings constructed with AAC, proper design provisions and codes are required.

Figure 1.1: Sample of a good application of AAC in USA

This research project forms part of the joint research program supported by Türkiye Gazbeton Üreticileri Birliği (TGÜB), and carried out at the Structural Mechanics Laboratory of the Middle East Technical University (METU), and Istanbul Technical University (ITU).

1.2 Background

1.2.1 Description of Autoclaved Aerated Concrete

Autoclaved Aerated Concrete (AAC) is a lightweight cellular material commonly used for production of masonry AAC units. It is composed of Portland cement, finely grouted silica sand, lime, gypsum, fly ash, water, and aluminum powder as an aerating agent [Costa et al., 2011]. Fly ash can be replaced instead of fine sand [Chusid, 1999].

In one of the most common methods for production AAC, all the dry materials are mixed and water is added to form the slurry. In the next step, aluminum powder is added to the slurry as an expansive agent. The reaction of aluminum powder with alkaline cement causes microscopic hydrogen bubbles to form, and increases the volume of the slurry by two or three times within 3 hours. Reaction of the quicklime with the water, creates the adequate heat to accelerate the initial set of Portland cement [Wittman, 1993]. In this step, after evaporation of hydrogen, the mixture is self-supporting and aerated concrete is cut into desired sizes and shapes by prestressed steel wires [Tanner, 2003]. The blocks are cured in pressured chamber, known as autoclave, for 11-12 hours under a pressure of 12 bars and a temperature of about 190-200°C, to achieve the desired structural properties.

Because of the fine cellular structure of the final produced material, it is an airtight, non-toxic, non-combustible, fire resisting, energy efficient, high quality and lightweight material which is about one-fifth to one-third the density of the conventional concrete [Penna et al., 2015]. Simple AAC manufacturing process, and cellular structure of the AAC can be seen in Figures 1.2[2] and 1.3[3].

[2] Hebel-USA, `http://www.hebel-usa.com/en/content/production_process_2555.php`, last visited on August 2016

[3] Wikipedia, the free encyclopedia, `https://en.wikipedia.org/wiki/Autoclaved_aerated_concrete`, last visited on August 2016

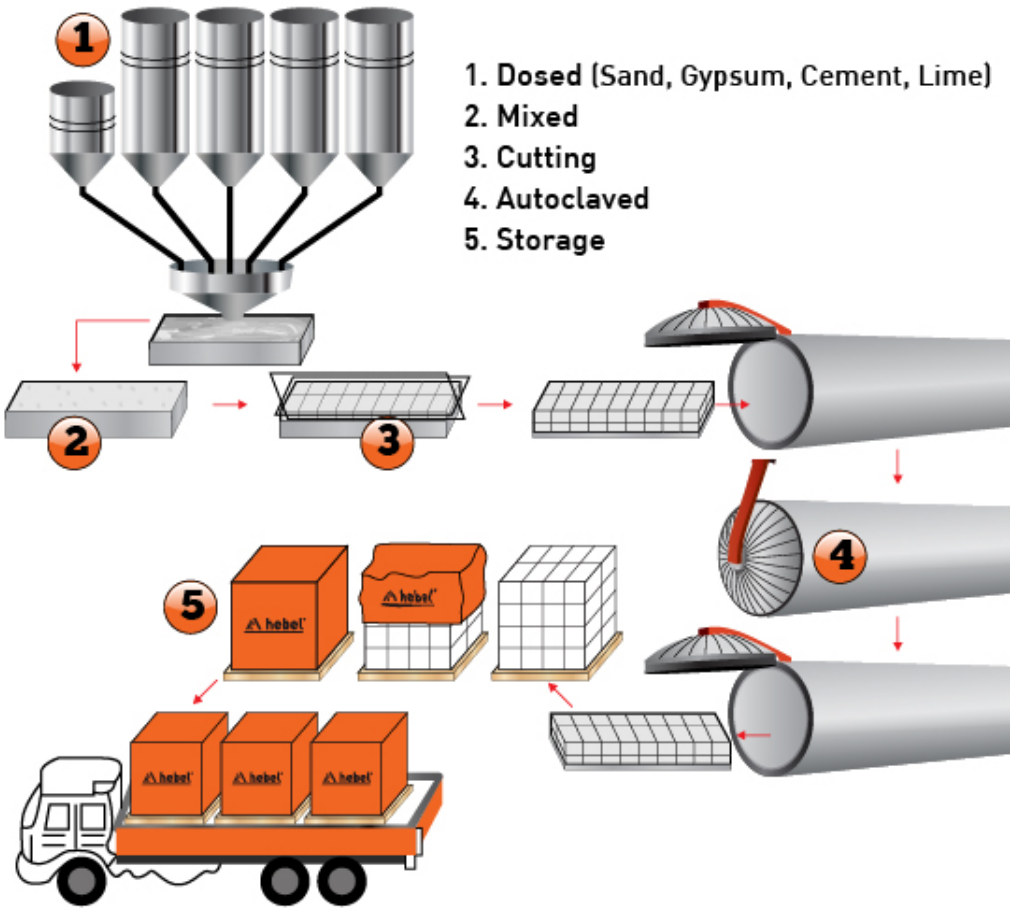

Figure 1.2: AAC manufacturing process

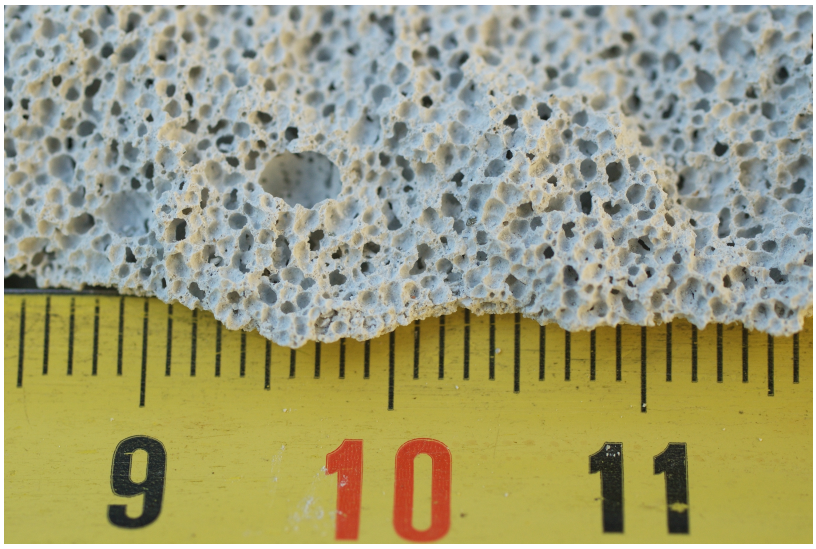

Figure 1.3: Cellular structure of AAC

1.2.2 Physical Characteristics of AAC

AAC's density is about one-third of the typical concrete and making it as a light weight material for constructions. The compressive strength of the AAC is about one-third of the typical concrete. Lower thermal conductivity of AAC compared to typical concrete (about one-eighth or less), makes the AAC an energy efficient material [Argudo, 2003].

In places where fire safety is important, AAC is very useful because of its higher fire resistance in comparison with typical concrete. Because of its internal porous structure, AAC has very low sound transmission and potentially useful acoustically. In Table 1.1, fire rating, mechanical and thermal characteristics of AAC are compared with typical concrete [Narayanan and Ramamurthy, 2000, Kim et al., 2003].

Table 1.1: Physical characteristics of AAC

Characteristics	**AAC**	**Typical concrete**
Density, (kg/m^3)	300 - 1000	1280 - 2400
Compressive strength, (MPa)	1.5 – 10	6.9 – 69
Thermal conductivity, (W/m°K)	0.07 – 0.26	1.4 – 3.6
Fire rating, (hours)	≤ 8	≤ 6

1.2.3 Autoclaved Aerated Concrete Parameters

The basis material properties of Aerated Autoclaved Concrete is presented as below according to [TS 12602, 2015], "Prefabricated Reinforced Components of Autoclaved Aerated Concrete".

1.2.3.1 AAC Compressive Classes

AAC is produced in different densities and compressive strengths. In Table 1.2, different strength classes of AAC is presented. For each of strength classes, corresponding compressive strength is provided.

Table 1.2: Compressive strength classes for AAC

Strength class	**Compressive strength, MPa**	**Strength class**	**Compressive strength, MPa**
AAC 1.5	1.5	AAC 5	5
AAC 2	2	AAC 6	6
AAC 2.5	2.5	AAC 7	7
AAC 3	3	AAC 8	8
AAC 3.5	3.5	AAC 9	9
AAC 4	4	AAC 10	10
AAC 4.5	4.5		

1.2.3.2 Tensile Strength and Flexural Strength

The manufacturer shall declare the flexural strength by tests. In the absence of the test results an estimate of the tensile strength or flexural strength can be obtained from the equations 1.1, 1.2, 1.3 and 1.4.

$$f_{ctk;\ 0,05} = 0.10 f_{ck} \tag{1.1}$$

$$f_{ctk;\ 0,95} = 0.24 f_{ck} \tag{1.2}$$

$$f_{cflk;\ 0,05} = 0.18 f_{ck} \tag{1.3}$$

$$f_{cflk;\ 0,95} = 0.96 f_{ck} \tag{1.4}$$

where

$f_{ctk;\ 0,05}$ = characteristic value of 5 %-quantile of axial tensile strength

$f_{ctk;\ 0,95}$ = characteristic value of 95 %-quantile of axial tensile strength

$f_{cflk;\ 0,05}$ = characteristic value of 5 %-quantile of flexural strength

$f_{cflk;\ 0,95}$ = characteristic value of 95 %-quantile of flexural strength

f_{ck} = characteristic value of compressive strength (see 1.2.3.1)

1.2.3.3 Modulus of Elasticity

In absence of test results, a mean value of the modulus of elasticity can be obtained as follows:

$$E_{cm} = 5(\rho_m - 150) \tag{1.5}$$

where

E_{cm} = mean value of the modulus of elasticity of AAC, MPa

ρ_m = mean value of the dry density of AAC, kg/m^3

1.2.3.4 Density, Shrinkage and Creep Classes

Density classes, drying shrinkage classes and creep classes are given in Table 1.3, 1.4 and 1.5.

Table 1.3: Density classes

Density class	**Mean dry density ρ_m, kg/m³**	**Density class**	**Mean dry density ρ_m, kg/m³**
300	> 250 ≤ 300	700	> 650 ≤ 700
350	> 300 ≤ 350	750	> 700 ≤ 750
400	> 350 ≤ 400	800	> 750 ≤ 800
450	> 400 ≤ 450	850	> 800 ≤ 850
500	> 450 ≤ 500	900	> 850 ≤ 900
550	> 500 ≤ 550	950	> 900 ≤ 950
600	> 550 ≤ 600	1000	> 950 ≤ 1000
650	> 600 ≤ 650		

Table 1.4: Drying shrinkage classes for AAC

Drying shrinkage class	**0.15**	**0.20**	**0.25**	**0.30**	**0.35**	**0.40**
ϵ_c mm per m	≤ 0.15	≤ 0.20	≤ 0.25	≤ 0.30	≤ 0.35	≤ 0.40

Table 1.5: Creep classes

Creep class	**0.5**	**0.6**	**0.7**	**0.8**	**0.9**	**1.0**
Mean creep coefficient	> 0.4	> 0.5	> 0.6	> 0.7	> 0.8	> 0.9
$\boldsymbol{\phi}$ **(**$\boldsymbol{t_0}$**,** $\boldsymbol{t_\infty}$**)**	≤ 0.5	≤ 0.6	≤ 0.7	≤ 0.8	≤ 0.9	≤ 1.0

1.2.3.5 Poisson's Ratio

Poisson's ratio for elastic strains shall be taken as 0.2. If cracking is permitted in AAC in tension, Poisson's ratio may be taken as 0.0.

1.2.4 AAC as Structural Elements

Different reinforced or unreinforced AAC panels are used as structural elements. Unreinforced AAC masonry blocks, reinforced vertical and horizontal wall panels, floor panels, roof panels, lintels, beams and other shapes can be used in variety of applications including industrial and residential constructions. The AAC wall panel units can be used as load bearing or non-load bearing walls inside or outside of the buildings. Moreover, reinforced floor or roof panels can be used efficiently as horizontal diaphragms for transmitting loads to the walls. Different types of AAC structural elements can be seen in the Figure 1.4[4].

AAC blocks are typically produced 200 $mm \times 600$ mm in plan, and thickness varies between 100 mm to 300 mm. Wall, roof and floor panels are mostly 200 mm by 600 mm, with a maximum length of 6 m.

In order to construct shear walls, vertical or horizontal panels are used. Furthermore, longitudinal reinforcements are placed at the end of panels in cores filled with grout. AAC structural walls are the most important elements in AAC structure to resist lateral forces or earthquakes.

[4] `http://www.masonrymagazine.com/using-autoclaved-aerated-concrete-correctly/`

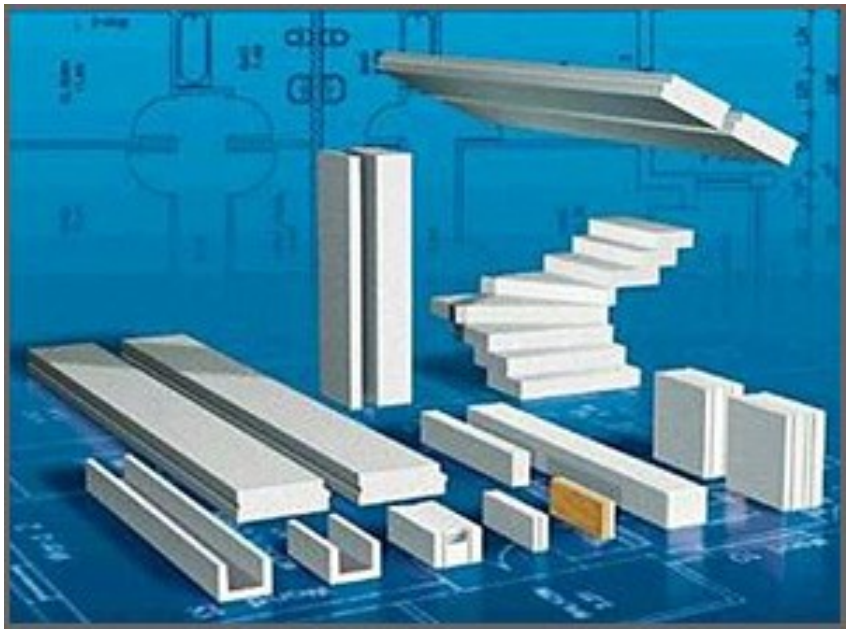

Figure 1.4: Different types of AAC structural elements

1.2.5 Mortar

Mortar is used as an adhesive to fix the AAC panels to each other, and provide bond to the longitudinal reinforcements between the panels. The cross section of joints between the panels is circular with 50 mm diameter, which is filled with a flowable fine grout mortar. This mortar is different from the typical mortar that is used in masonry structures. It is a liquid mixture of Portland cement, fine sand, water and some other admixtures like, latex or water retentions.

1.2.6 AAC Walls Construction Process

First, the surface of the foundation is roughened and leveled to have a smooth place to start the construction of AAC vertical walls. The spacing of the vertical reinforcement between panels should be precisely ensured. The AAC vertical wall panels are placed between the longitudinal reinforcements, stabilized and guided into the place. Temporary bracing is installed to stabilized the panels and remains in place until the concrete girder is hardened enough. Next, the flowable fine grout mortar is filled into the cells between the panels to complete

installation. After one day, the excess mortar is scraped and the top girder of panels is constructed.

1.3 Literature Review

In this section, a short literature review of the previous researches on AAC shear wall is presented.

Most of the prior researches on AAC shear walls have been carried out on the behavior of the walls constructed by masonry type AAC blocks. In a research by [de Vekey R. C. et al., 1986] the effects of specimen dimension, moisture and thickness on flexural capacity of the walls under lateral forces is investigated. This study deducted that under the loads perpendicular to the bed joints, the flexural capacity of the specimens decreased as the thickness or the moisture increased. Also, when the dimensions of the units decreased, the flexural capacity increased. It is mentioned that the results were almost the same when the applied load was parallel to the bed joints.

In another research by [Al-Shaleh and Attiogbe, 1997] the out of plane flexural strength behavior of non-load bearing masonry AAC walls built by blocks was studied. The main objective of this study was to investigate the behavior of flexural capacity of walls in running bonds parallel or perpendicular to the bed joints. This study indicated that the out-of-plane flexural capacity of the AAC walls was almost the same parallel or perpendicular to the bed joints.

In a research by [Brightman, 2000] at University of Texas at Austin, 2 AAC shear wall specimens constructed with horizontal panels were tested to examine the in-plane behavior of shear walls. From the experimental results, improvements to the construction techniques and testing procedures were offered. Furthermore, enhancements for existing design models made from the preliminary information acquired on the behavior of shear-dominated AAC shear walls. Based on the results, the researcher mentioned also that based on the results, AAC can be safely be used throughout United States.

Another research project at University of Texas at Austin, by [Varela et al., 2004] consisted of 14 AAC shear wall specimens, and a two-story, full scaled AAC assemblage structure, which was tested under reverse cyclic lateral loads. Details about the tests are presented in Table 1.6, 1.7, and 1.8. The experimental results along with the numerical simulations were used to calculate the values for response modification coefficient (R) and deflection amplification factor (C_d). From the tests, this study proposed conservative limits for displacement ductility capacity and drift ratio capacity for flexure dominated AAC shear wall systems. After the numerical simulations, $R = 3$ and $C_d = 3$, were selected to use in seismic design of AAC shear wall systems in the United Stated [Varela, 2003].

Table 1.6: Summary of the tests at University of Texas at Austin

Specimen	**Failure mode**	**AAC units**	**Material supplier**	$\mathbf{f'_{AAC}}$ **(MPa)**
2	Shear	Vertical Panels	Ytong	N.A.
15a	Flexure	Vertical Panels with Blocks	Babb	7.9
15b	Flexure	Vertical Panels with Blocks	Babb	7.9
16	Flexure	Vertical Panels with Blocks	Babb	7.9

Table 1.7: Geometry and reinforcement specifications of tests at University of Texas at Austin

Specimen	**L (m)**	**H (m)**	**T (m)**	**Aspect ratio**	**Reinforcement**	
					Exterior	**Interior**
2	6.1	3.9	0.20	0.64	2-B7 25 mm 0.6 m from ends	No
15a	2.8	3.9	0.25	1.38	No	16 mm, 0.2 m from ends
15b	2.8	3.9	0.25	1.38	No	16 mm, 0.2 m from ends
16	2.8	3.9	0.25	1.38	No	16 mm, 0.2 m from ends

In a research project by Hebel International in Germany [Tanner et al., 2004], 12 AAC shear wall specimens were tested under in-plane lateral loads and varying axial load, to observe the behavior of AAC walls with sliding resistance. The dimensions of all test specimens were 2.5 m by 2.5 m, with an aspect ratio of 1.0. It was concluded that for walls with sliding resistance, web shear cracking

Table 1.8: Applied axial load details of tests at University of Texas at Austin

Specimen	**Exterior reinforcement (kN)**	**Load maintainer (kN)**	**Self-weight loading beam (kN)**	**Total (kN)**
2	117.9	480.4	35.6	639.9
15a	0.0	90.0	22.2	111.2
15b	0.0	90.0	22.2	111.2
16	0.0	90.0	22.2	111.2

was the major failure mode in all the specimens [Tanner, 2003].

A series of tests were carried out on full scale Ytong AAC infilled walls by Building Research Institute (NISI) in Sofia, Bulgaria. Totally, 9 confined AAC shear wall specimens were tested, while 6 of the specimens contained opening. The study indicated that confined AAC masonry is practical for 1 to 3 story load resisting structures [Building Research Institute (NISI), 1997].

1.4 Objective and Scope

The objective of this research is to:

- understand the behavior of AAC reinforced panel walls
- determine the ductility, strength, and failure mode for typical walls by testing
- compare existing design equations and Turkish Code proposals with test results.

For this purpose a research programme consisted of tests, analysis and code comparison was planed. The testing phase of the dissertation evaluated the 6 AAC shear wall specimens with different aspect ratios (ratio of height to length) varying between 0.7 and 2.2, and varying applied axial load between 0 and 0.5 *MPa*. AAC shear walls were constructed with AAC reinforced panels laid side by side vertically. In the analytical phase of this research, design provisions were

tried to be verified by means of experimental results.

1.5 Organization of Dissertation

This research embraces both experimental and analytical phases of AAC shear wall panels. Introduction and background information about Autoclaved Aerated Concrete are provided in Chapter 1. Chapter 2 provides testing programme and test setup. In Chapter 3, experimental results for each AAC shear wall specimen are presented. Evaluation of the test results is given in Chapter 4. Chapter 5 contains the conclusion of this dissertation.

CHAPTER 2

EXPERIMENTAL PROGRAM

2.1 General

In this chapter the experimental program of this study is explained in detail. All experimental information such as, properties of each AAC test specimen, test setup, loading equipment, instrumentation, and data acquisition along with loading protocol is provided hereinafter.

The objective of the tests was to determine the behavior of AAC wall panels. Reinforced vertical AAC wall panels can be used as load-bearing walls in masonry constructions. These panels can be used both as interior and exterior walls. Six specimens with different arrangements were tested. The reinforcement ratio, axial load, and geometry were selected as the test parameters compatible with the objectives of the tests. To study the effect of different aspect ratios in AAC vertical wall panel capacity, the number of panels was changed in testing program. Tests were conducted with and without axial load to determine the influence of axial force in the capacity of AAC walls. Specimens with two and four vertical wall panels were tested with and without axial load. A test without axial load and another test with a window opening were carried out for specimens with six AAC wall panels. The height of all the specimens were 2.4 m and since one panel measures 0.6 m the length of specimens with two, four and six units were 1.2 m, 2.4 m and 3.6 m, respectively.

Specimens were constructed by installing different number of AAC vertical wall panels laid side by side vertically. In Table 2.1, details of the specimens are

presented. N_0 in the table is axial load capacity of the section which is equal to $f_c A_g$ excluding the longitudinal bars. The axial load applied to specimens PN2 and PN4 was approximately 0.5 *MPa* as given in Table 2.2.

Table 2.1: AAC wall dimensions

Specimen	**Number of panels**	**L (mm)**	**H (mm)**	**T (mm)**	**N/N_0**
PN1	2	1200	2400	200	0.00
PN2	2	1200	2400	200	0.13
PN3	4	2400	2400	200	0.01
PN4	4	2400	2400	200	0.13
PN5	6	3600	2400	200	0.02
PN6	6	3600	2400	200	0.02

Table 2.2: Details of applied axial load

Specimen	**Axial load (kN)**	**Self-weight & beam (kN)**	**Total axial load (kN)**	**Axial stress (MPa)**
PN1	0	6.22	6.22	0.02
PN2	120	6.22	126.22	0.52
PN3	0	12.44	12.44	0.02
PN4	240	12.44	252.44	0.52
PN5	0	18.66	18.66	0.02
PN6	0	16.68	16.68	0.02

2.1.1 Material Properties

Material properties of specimens are provided in the following section. The properties for AAC wall panels and steel are determined by the laboratory tests. For all tests, the materials used were exactly the same.

2.1.1.1 AAC Wall Panels

Reinforced AAC wall panels are produced in the factory and delivered to the Structural Mechanic Laboratory. The height, length and thickness of each panel are 2400 *mm*, 600 *mm* and 200 *mm*, respectively. Specifications and interior

reinforcement of the panels which are used in this study are given in the Table 2.3 and Figure 2.1.

Table 2.3: Physical properties of G4 wall panels

G4 Panel type	**Dry density (kg/m^3)**	**f_c (MPa)**	**E (MPa)**
Type 1	600	4	2250
Type 2	700	4	2750

2.1.1.2 Steel

Longitudinal bars with 8 *mm* diameter and to get flexural strength, 3 *m* length were used to fix the panels to the foundation, and to avoid slipping of the AAC panels. Bars with 16 *mm* and 8 *mm* diameters were used as compression and tension steel, and as stirrups, respectively in the reinforced top loading beam. The yield strength was 413 *MPa* and ultimate strength was 545 *MPa*. Stress-Strain test results of 8 *mm* steel bars can be seen in Figure 2.2.

2.1.2 Construction of the Specimen

The following construction procedures was followed in the METU Structural Mechanics Laboratory:

- A strong foundation was prepared as shown in Figure 2.3.
- Bars between the panels were placed into the foundation before foundation concreting; so there were no lap splices for the rebars
- AAC vertical wall panels were installed on the foundation. It should be noted that no base leveling mortar was used during the construction of specimens, and panels were put directly on the concrete foundation.
- The joints/grooves with longitudinal steel between the vertical panels were filled by flowable cement mortar

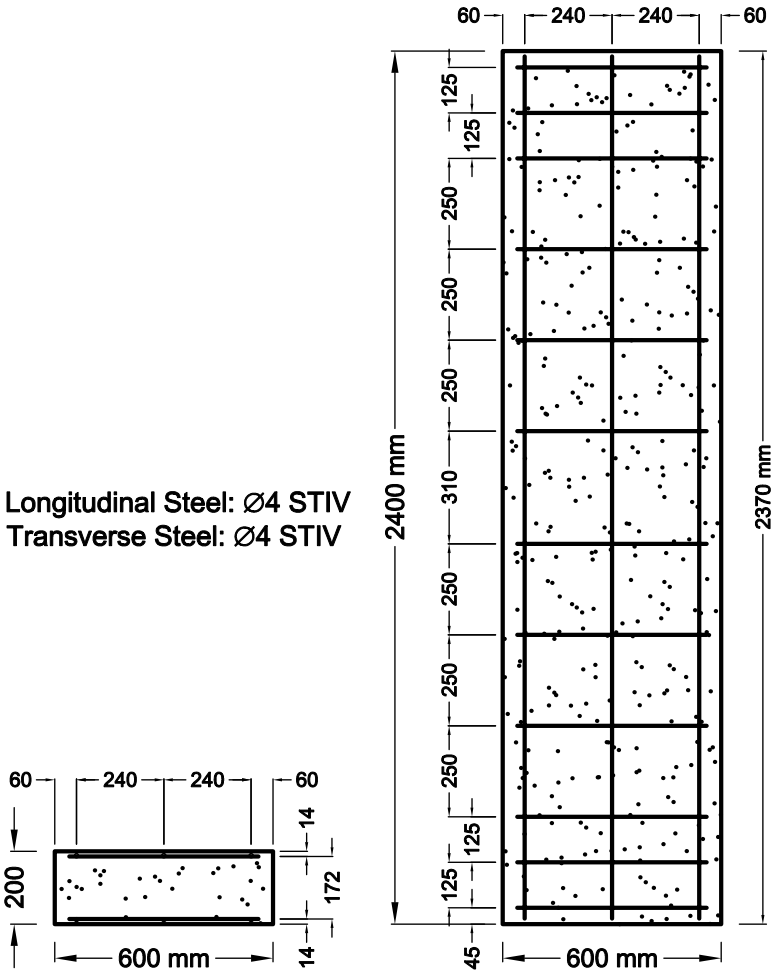

Figure 2.1: Interior reinforcement of the panel

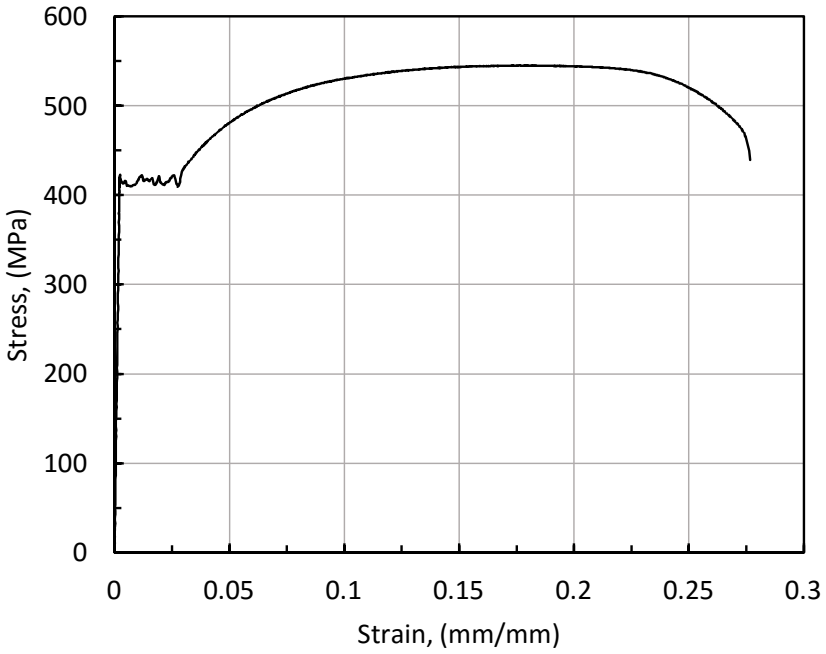

Figure 2.2: Stress-strain test result of $\phi 8$ rebar

- In order to mimic the real panel wall applications, a reinforced concrete top girder was put on the panels. The rebars which were anchored directly to the foundation and passes between panels were fixed into the top girder
- Specimens were white washed to ease observing the cracks.
- Measuring instruments were installed in the predetermined locations to gather the required data. For details about instrumentation see section 2.3.1.

2.1.3 Specimen 1, PN1

The PN1 specimen was constructed with two vertical wall panels and tested without axial load as shown in Figure 2.6. The wall system measured 1.2 m long, 2.4 m high (top of foundation to bottom of the loading beam), and 200 mm thick as shown in Figure 2.5. For the full contact of the AAC panels to the foundation, the surface of the foundation was smoothened and two panels were placed on the foundation. The longitudinal reinforcement of this sample consisted of three S420 bars with 8 mm diameter, placed 600 mm apart from

Figure 2.3: Preparation of the foundation

each other. This reinforcement was selected to provide required flexure strength. The longitudinal bars were anchored properly into the foundation and loading beam, with 90° hooked ends to avoid slip. In order to connect the panels to each other and to make the panels to behave as a unit wall, the groove between the panels with $\phi 8$ rebar was filled with a proper mortar as shown in Figure 2.4.

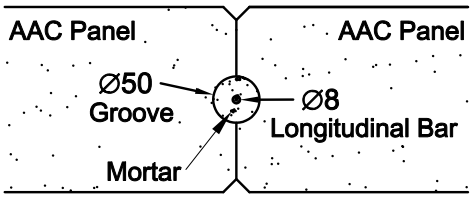

Figure 2.4: Top view of the joint between panels

2.1.4 Specimen 2, PN2

Construction procedure and the geometry of the specimen PN2 were exactly the same as the specimen PN1. However, a constant axial load of 126.2 kN was applied throughout the test. Specimen 2 was constructed with two vertical AAC wall panels. The wall measured 1.2 m long by 2.4 m high (top of foundation to bottom of the loading beam) by 200 mm thick. The longitudinal rods of the specimen placed 600 mm from each wall end. In the Figures 2.7 and 2.8 a simple sketch of the specimen and final view of the specimen PN2 can be seen.

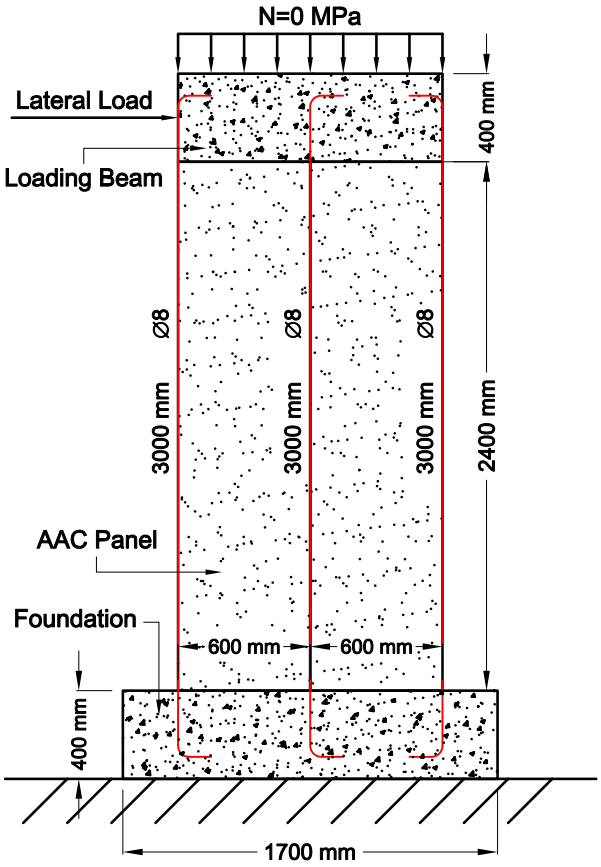

Figure 2.5: Dimensions and bars position of PN1 specimen

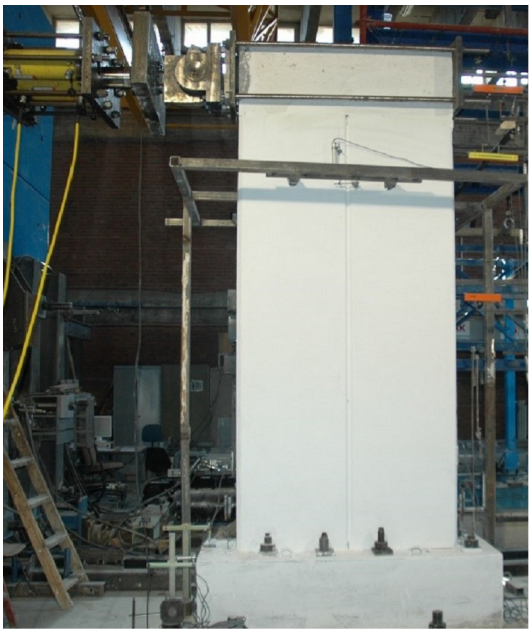

Figure 2.6: Final view of PN1 specimen

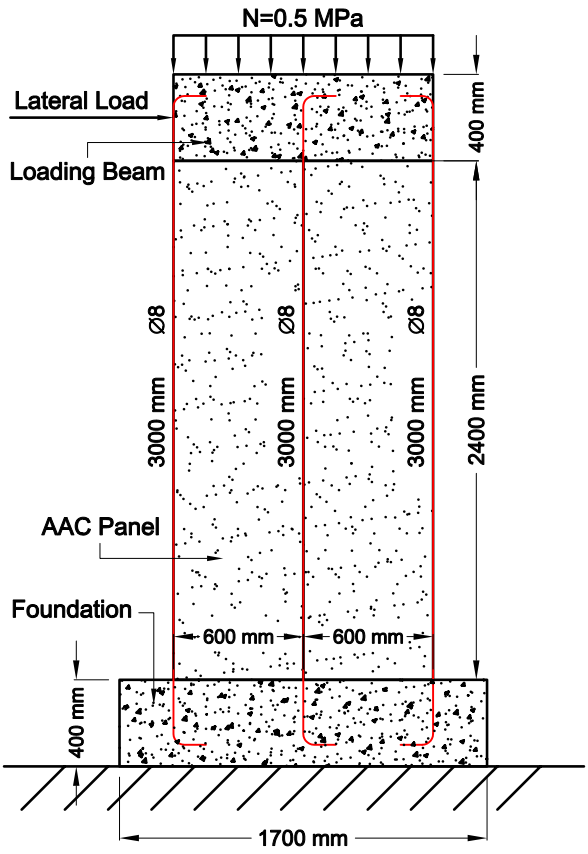

Figure 2.7: Dimensions and bars position of PN2 specimen

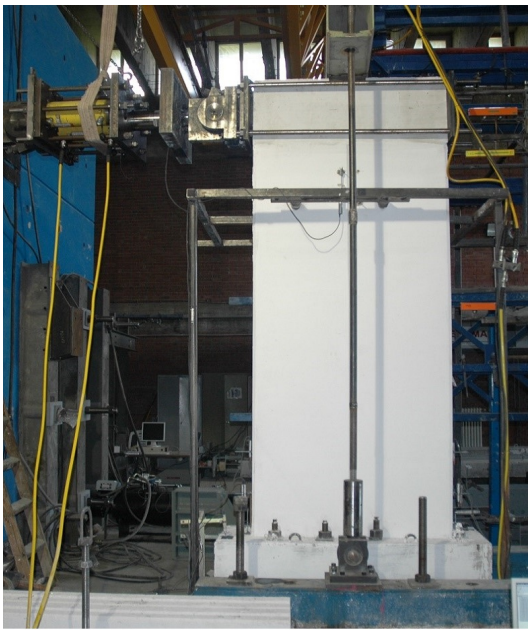

Figure 2.8: Final view of PN2 specimen

2.1.5 Specimen 3, PN3

The construction procedure of Specimen 3 was exactly the same as other specimens. Specimen 3 was constructed with four vertical AAC wall panels. The PN3 Specimen test was carried out without an axial load. The dimensions were 2.4 m long by 2.4 m high (top of foundation to bottom of the loading beam) by 200 mm thick. The longitudinal bars of the specimen were placed 600 mm apart from each other. In Figure 2.9 and 2.10, a simple sketch of the specimen and final view of the Specimen PN3 is shown.

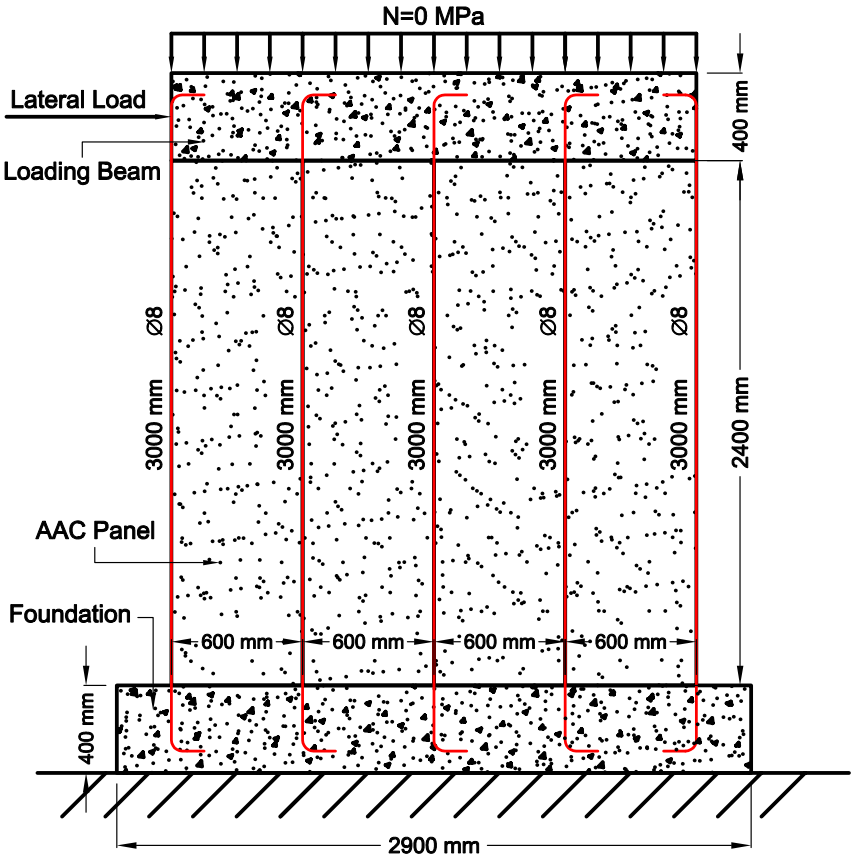

Figure 2.9: Dimensions and bars position of PN3 specimens

2.1.6 Specimen 4, PN4

Specimen PN4 were exactly in the same dimensions as Specimen PN3 except the axial load. A constant axial load of 252.4 kN was applied throughout the

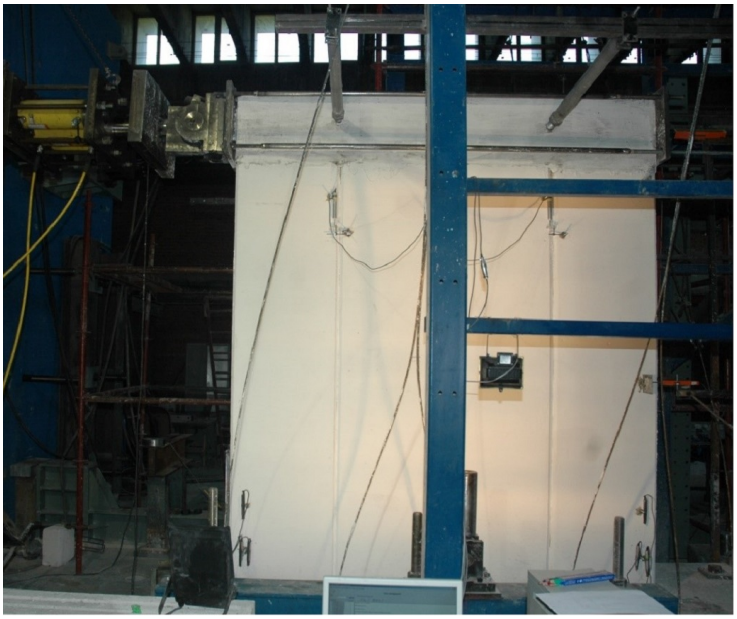

Figure 2.10: Final view of PN3 specimen

test on this specimen. Specimen 4 was constructed with four vertical AAC wall panels. The dimensions were 2.4 m × 2.4 m × 0.2 m, and five $\phi 8$ bars were placed 600 mm apart. In Figures 2.11 and 2.12, simple sketch and final view of the specimen PN4 can be seen.

2.1.7 Specimen 5, PN5

The same construction procedure was followed in this specimen. The PN5 was constructed with six vertical AAC wall panels. PN5 Specimen test was carried out without axial load. The wall measured 3.6 m long, 2.4 m high (top of foundation to bottom of the loading beam), and 200 mm thick. The longitudinal bars were placed 600 mm apart from each other due to the width of panels. In Figures 2.13 and 2.14, dimensions of the and a general view of the specimen is given.

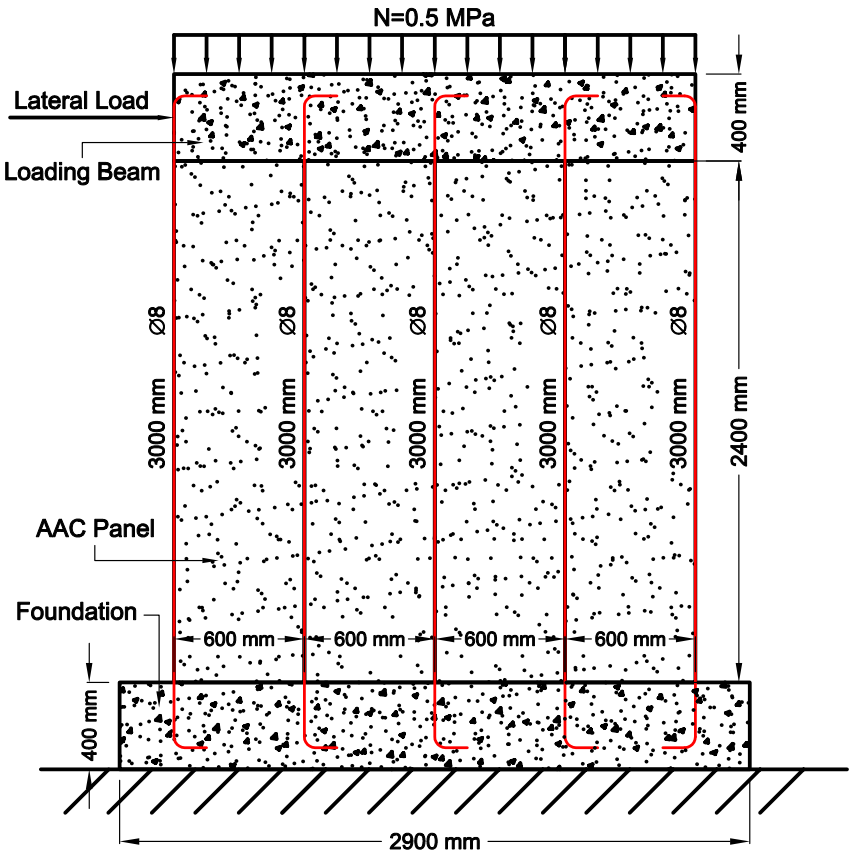

Figure 2.11: Dimensions and bars position of PN4 specimen

Figure 2.12: Final view of PN4 specimen

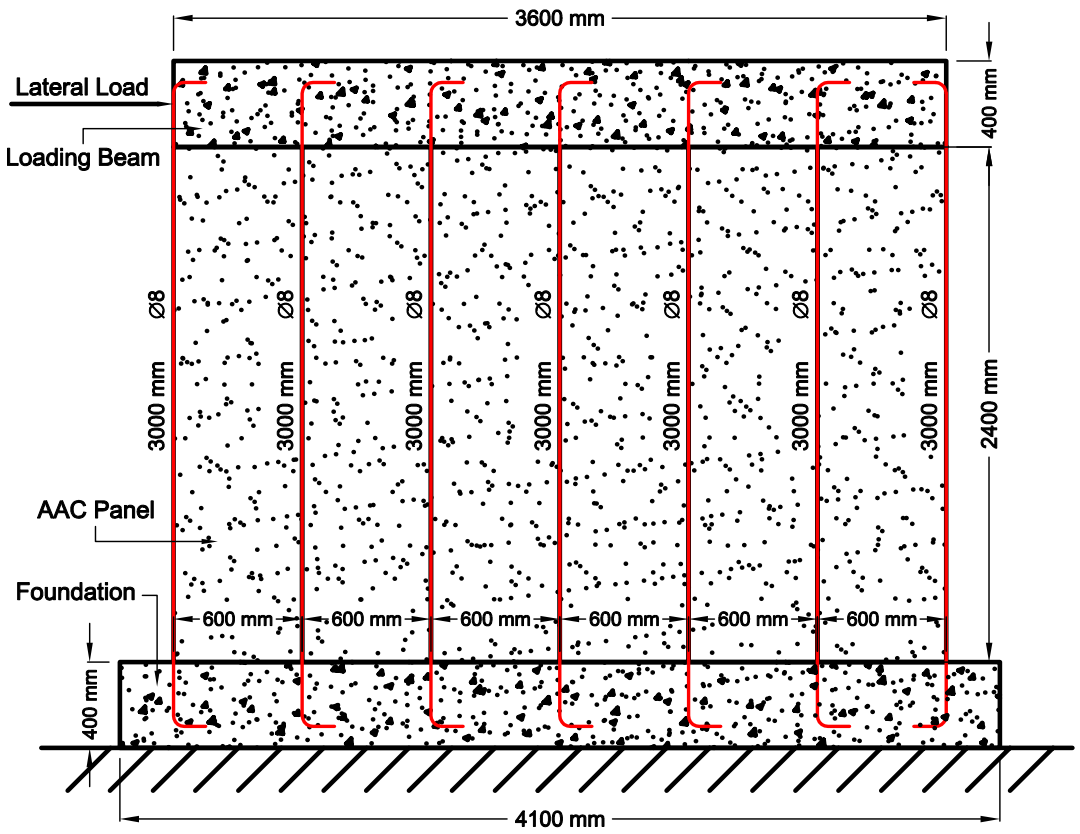

Figure 2.13: Dimensions and bars position of PN5 specimen

Figure 2.14: Final view of PN5 specimen

2.1.8 Specimen 6, PN6

Similar to other specimens, the same construction steps were employed to Specimen 6. The only difference compared to Specimen 5 was the window opening as shown in Figure 2.15. Specimen 6 was constructed with four full vertical AAC wall panels and two panels with 1.1 m height. The wall measured also 3.6 m long, 2.4 m high (top of foundation to bottom of the loading beam), and 200 mm thick. The window opening was 1.2 m $\times$ 1.2 m. The reinforced concrete loading beam on the window opening part was 100 mm deeper than the rest of girder. To fix the shorter panels in place, two steel angels attached the short panels to the full height panels at the bottom corners. The dimensions of the steel angels were 120 mm $\times$ 40 mm $\times$ 1.5 mm. A general view of the test of PN6 is given in Figure 2.17.

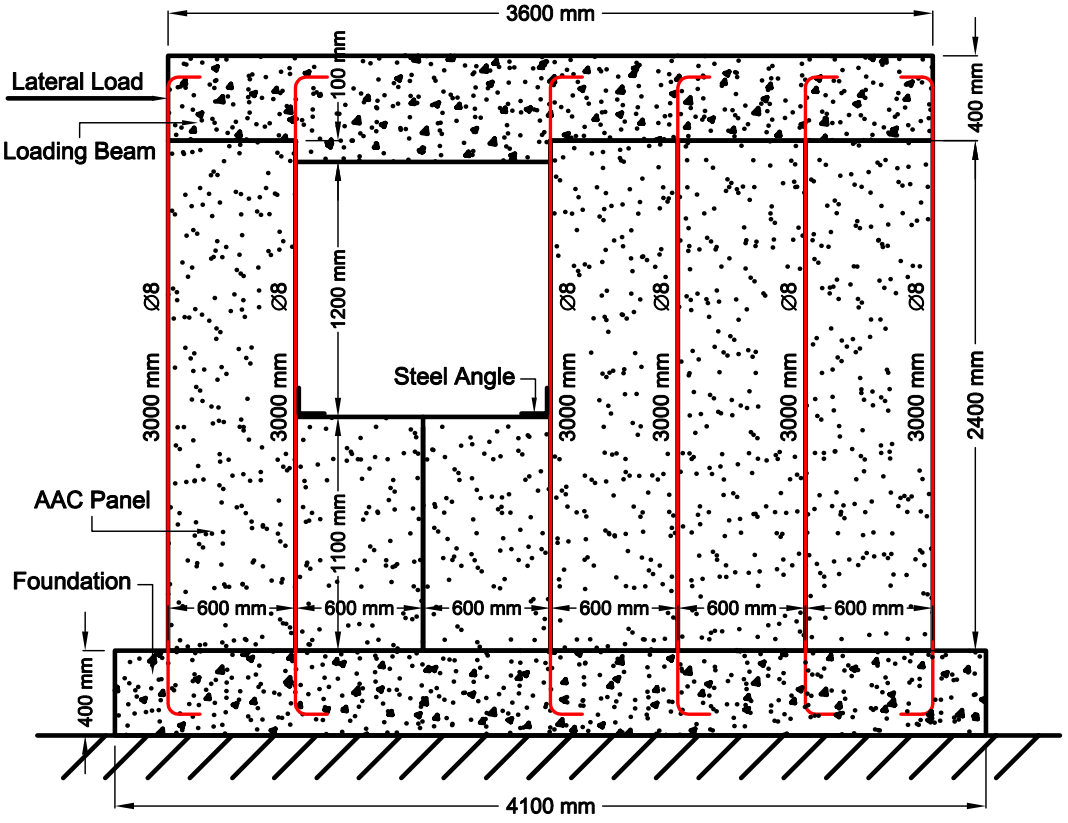

Figure 2.15: Dimensions and bars position of PN6 specimen

Figure 2.16: Steel angle brackets used at the lower corners of window opening

Figure 2.17: Final view of PN6 specimen

2.2 Test Setup

The specimens were tested using the setup presented in Figure 2.18. Different parts of the test setup will be described in the following sections.

2.2.1 Lateral Loading System

Lateral load was applied to the AAC panel wall system by means of hydraulic rams as shown in Figure 2.18. The hydraulic cylinders were pin connected both to the reaction wall and loading beam in order to prevent any accidental moment application to the specimens. A load cell was also attached to the tip of the ram to measure the applied lateral load.

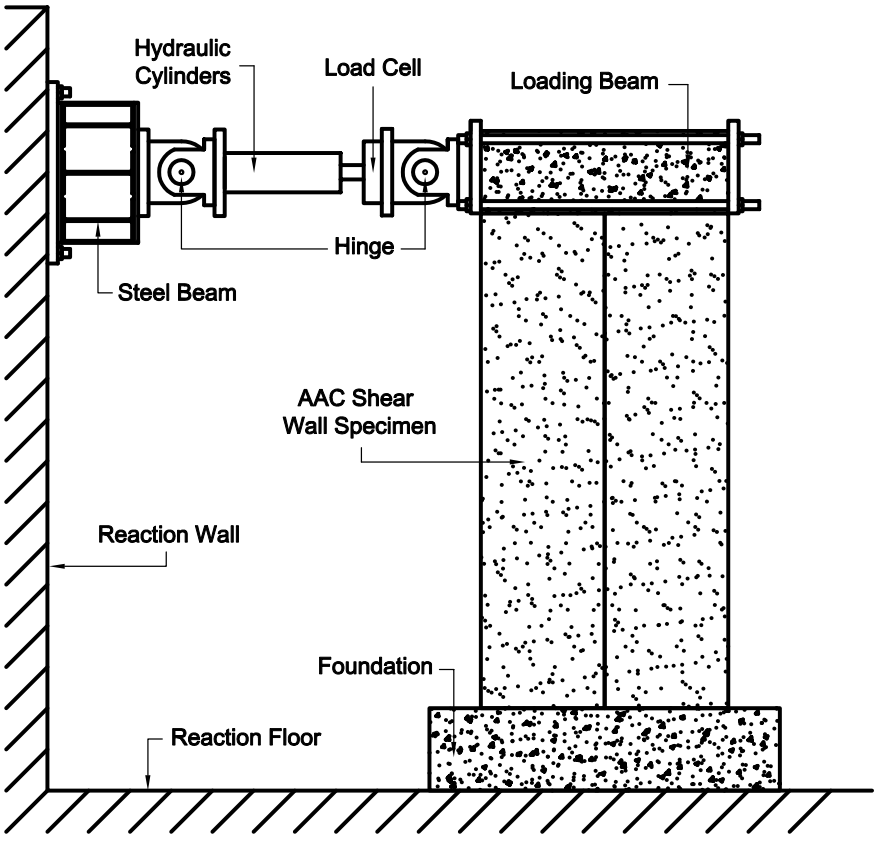

Figure 2.18: Typical test setup for applying lateral load

2.2.2 Axial Loading System

On the top of the PN2 and PN4 specimens, two vertical hydraulic rams were installed on a steel cross beam to apply the axial load. Axial load was applied to the specimens using two steel rods attached to the hydraulic actuators. As shown in Figure 2.19, the rods are passing through the cross beam, hydraulic rams, and load cells, and are locked at the top tip. The rods are hinges connected at the base to the steel beams which are also fixed to the strong floor. At the beginning of each test axial load was applied by the hydraulic rams and was tried to be kept constant during the tests. The load applied by the hydraulic rams and self-weight of the concrete loading beam on the top, was considered as the total axial load for each specimens.

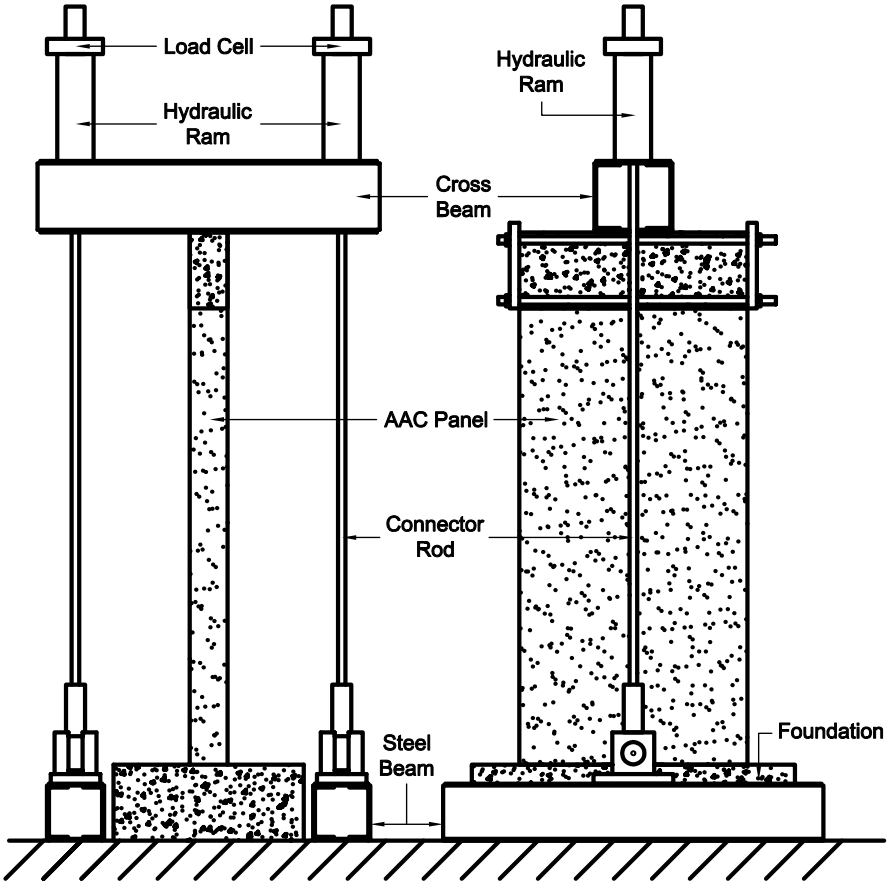

Figure 2.19: Setup for applying axial load

2.2.3 Loading Beam

A reinforced concrete beam was built on top of each specimen to distribute the applied lateral load uniformly to the vertical panels underneath. For the reinforcement of the girder, five 16 *mm* diameter compression and tension bars, and 8 *mm* bars at every 200 *mm* as stirrups were used. The cross section of the loading beam is shown in Figure 2.20. The loading beam was used to:

- allow lateral loading on the wall specimen
- enable application of axial loading on the wall system
- make possible installation of out-of-plane bracing system
- keep the vertical AAC wall panels together

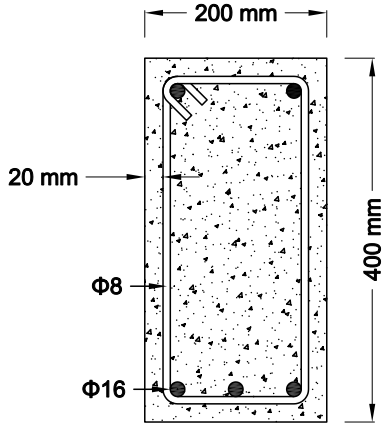

Figure 2.20: Cross section of the reinforced concrete loading beam

2.2.4 Foundation

A reinforced concrete foundation was built to enable construction of AAC wall system. The foundation was post-tensioned with high strength rods to the strong floor to prevent any sliding or uplifting during testing. A schematic view of the foundation is shown in Figure 2.21.

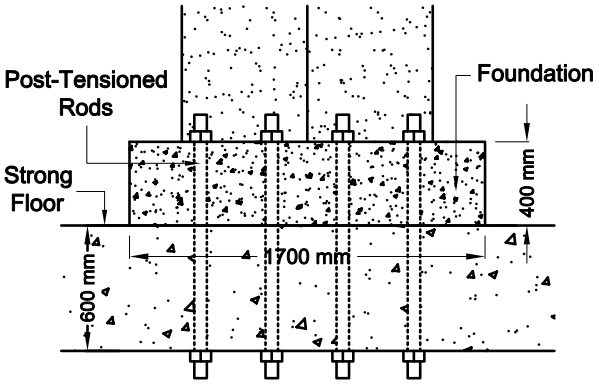

Figure 2.21: Reinforced concrete foundation

2.2.5 Bracing System

The lateral bracing system prevented the out-of-plane movement of the AAC wall panels. The system was made of steel frames and installed around the specimens. Two arms of the bracing system loosely touch with ball bearings to the top loading beam as shown in Figure 2.22. The lateral bracing system is clearly visible in every photographs of the specimens.

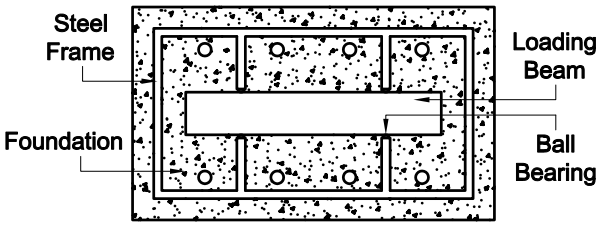

Figure 2.22: Top view of lateral bracing system

2.3 Data Acquisition and Instrumentation

2.3.1 Instrumentation

Behavior of the specimens are monitored by some measurement devices like LVDTs and Load Cells which are installed in predefined positions. The instrumentation included the followings:

- Load cell to measure:
    - applied lateral force
    - the axial load applied by hydraulic rams in PN2 and PN4
- Linear variable differential transformer (LVDT) or dial gauges to measure:
    - horizontal displacement at top, middle and bottom of the wall height
    - horizontal displacement at the mid height of the loading beam
    - slip between the AAC panels and foundation
    - slip between the foundation and reaction floor
    - vertical displacement of the specimen at different levels
    - vertical base displacement of the foundation
    - displacement of the AAC panels relative to each other

Details about the position of the LVDTs and the channel numbers of the gauges can be seen in the Figure 2.23.

2.3.2 Data Acquisition System

Data were acquired by a VISHAY Micro-Measurement 5100B scanner. Acquiring, reducing, presenting, and storing measurement data from instrumentations were carried out by StrainSmart software in a computer with Microsoft Windows® system.

2.4 Loading Protocol

The loading protocol for the in-plane lateral load of the specimens is shown in Figure 2.24. The loading history involved five increments and was consisted of series of reversed cycles. As can be seen in figure below, each displacement cycle was applied twice.

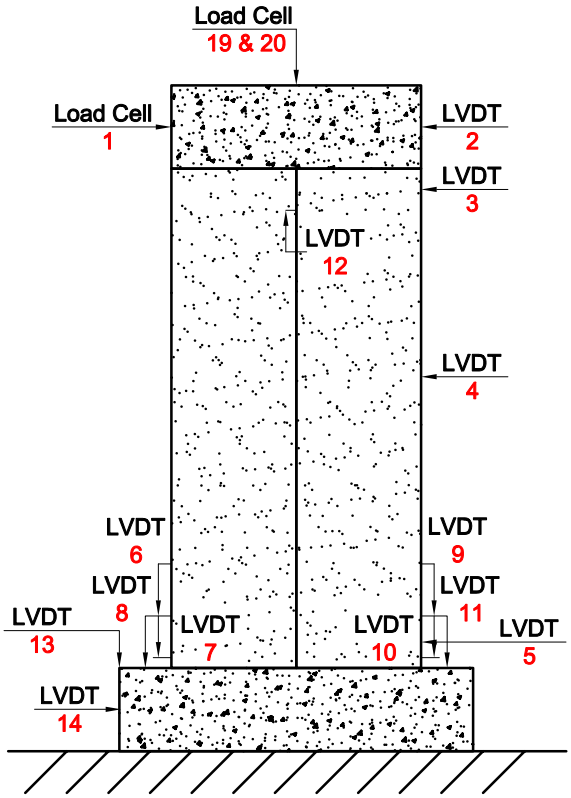

Figure 2.23: Instrumentation devices

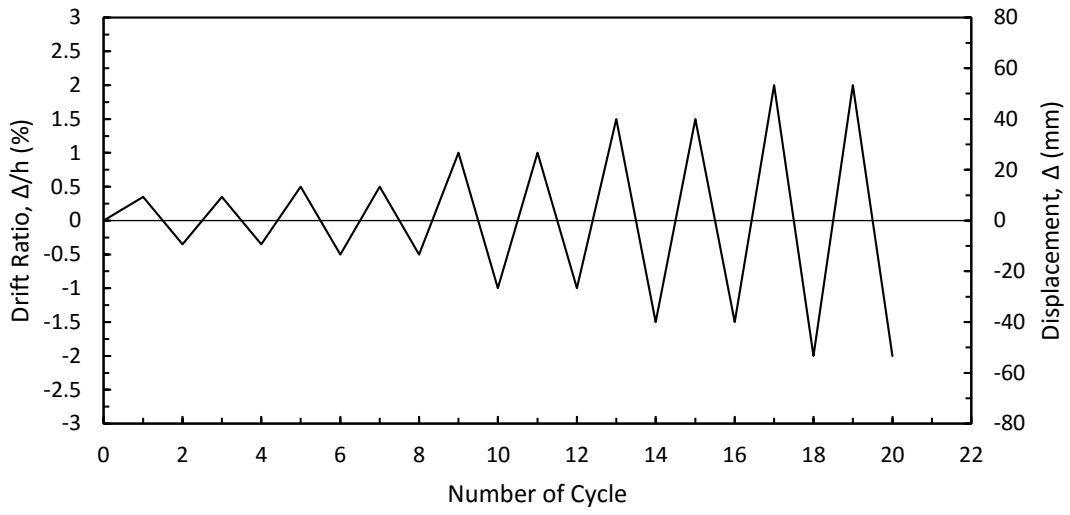

Figure 2.24: Loading history

CHAPTER 3

TEST RESULTS

3.1 Specimens

This chapter presents the behavior and test results of the six specimens. The load-displacement curves in this chapter present the applied in-plane lateral load versus the horizontal top displacement, percent drift ratios are also provided as secondary horizontal axis. The drift ratio was calculated at the level of the load application by dividing the horizontal displacement of the specimen measured by the LVDT to its height.

3.1.1 Specimen 1, PN1

In this specimen, test was carried out with two vertical panels without axial load as explained in section 2.1.3.The maximum forward and backward loads applied to the specimen were 18.7 kN and -16.2 kN, respectively, which were attained in the first cycle. The drift ratio corresponding to the maximum lateral loads is $\pm 0.35\%$. The applied lateral load versus displacement, and the base moment-curvature curves are indicated in the Figures 3.1 and 3.2.

The middle vertical longitudinal bar was confined by means of the two panels around it and by the mortar casted in the groove. However, at both ends of the wall system, the longitudinal vertical bars were guided in a half circular groove filled with mortar. Since end faces of the walls were not confined, the longitudinal bars tended prematurely buckle under compression.

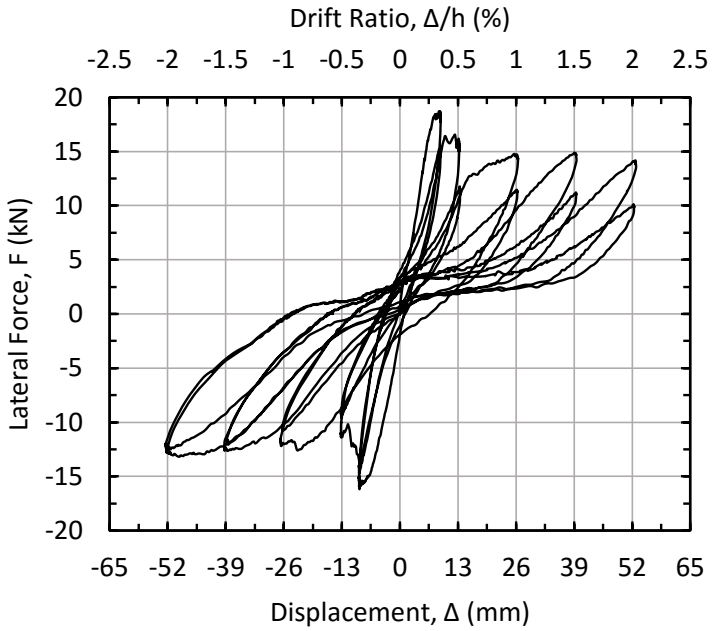

Figure 3.1: Specimen PN1 lateral load versus displacement and drift ratio

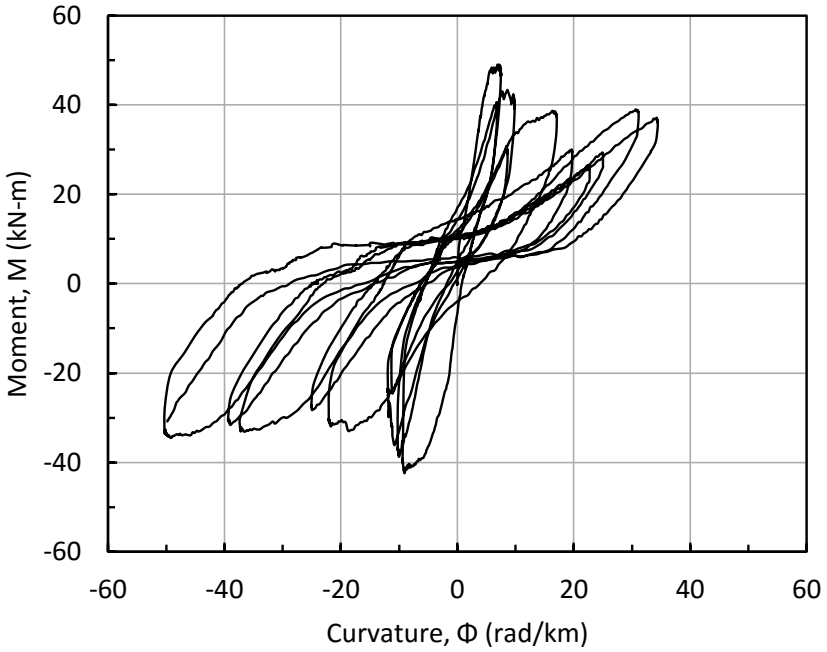

Figure 3.2: Specimen PN1 base moment-curvature

The cement mortar in the half groove of the bottom corner which is under compression in positive excursion was cracked at the 0.5% drift ratio. In the second cycle of the 0.5% drift ratio, the longitudinal bar under compression was bent as can be seen in the Figure 3.3. After the second cycle of the ±0.5% drift ratio, the lateral load capacity of the specimen reduced promptly about 20% to 14.8 *kN*, and -13 *kN*, and was almost constant up to 2% drift ratio. The load-displacement curve indicates the ductile behavior of the specimen. After the second cycle of the 1% drift ratio, width of the crack between two vertical panels increased. Bottom corners of the AAC wall panels crushed at the end of the test. All aforementioned damages are clearly illustrated in Figure 3.3.

3.1.2 Specimen 2, PN2

The test results of the PN2 specimen are presented in this section. Test was carried out with two vertical panels with axial load as explained in section 2.1.4. The maximum forward and backward loads applied to the specimen were 53 *kN* and -47.9 *kN* respectively. The drift ratio corresponding to the maximum lateral loads are 0.95% and -0.95%. The applied lateral load versus displacement, and the base moment-curvature curves are indicated in Figures 3.4 and 3.5. It should mention that one of the LVDTs shifted accidentally during the test and it resulted with an error in moment-curvature curve.

The capacity of the specimen started to decrease after 0.96% drift ratio. At ±1.4% drift ratios, the specimen capacity reduced to 41.2 *kN* and -35.2 *kN*, which are almost 20% of the maximum capacity of PN2 specimen. The longitudinal bar at compression side of the specimen buckled at 0.5% drift ratio. The bottom corners of AAC vertical wall panels crushed at the second cycle of 1.5% drift ratio. In PN1 specimen, the vertical joint between the panels widened and panels were not damaged excessively, whereas in PN2 specimen, owing to the axial load, bottom of the panels cracked horizontally and the panels did not slip. In Figure 3.6, failure pictures of the PN2 specimen are shown.

Figure 3.3: Specimen PN1 failure pictures

Figure 3.3: Specimen PN1 failure pictures (cont.)

Figure 3.3: Specimen PN1 failure pictures (cont.)

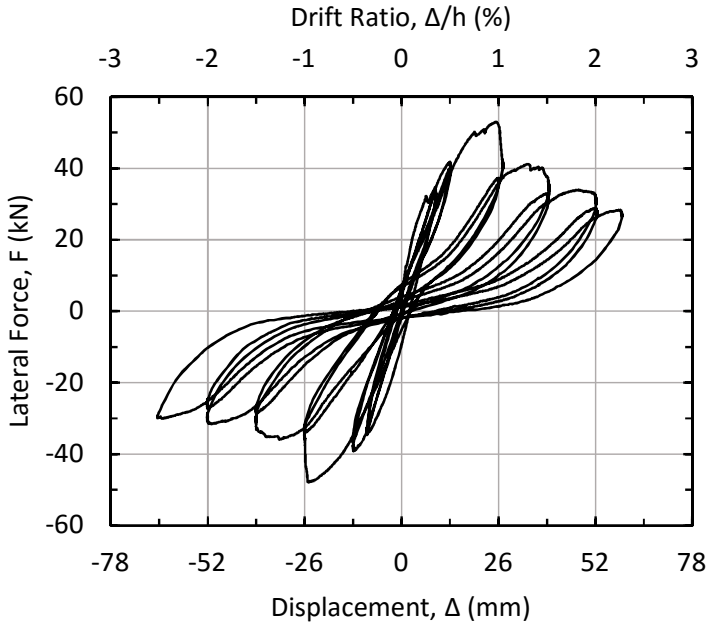

Figure 3.4: Specimen PN2 lateral load versus displacement and drift ratio

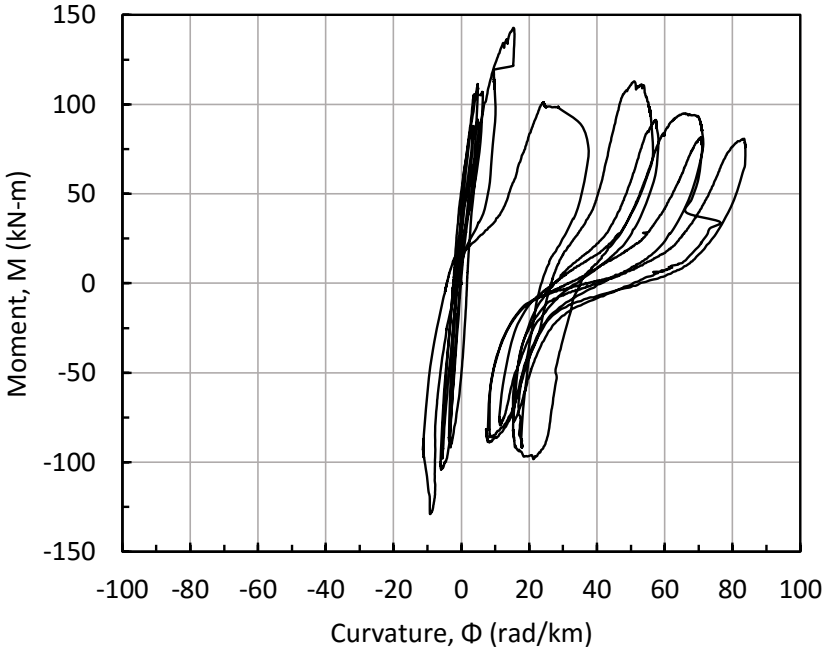

Figure 3.5: Specimen PN2 base moment-curvature

Figure 3.6: Specimen PN2 failure pictures

Figure 3.6: Specimen PN2 failure pictures (cont.)

3.1.3 Specimen 3, PN3

This section presents the test results of Specimen PN3. As explained in section 2.1.5, the test was carried out with four vertical panels and without axial load.

The maximum forward and backward loads applied to the specimen were 48 kN and -33.4 kN, respectively. The drift ratios corresponding to the maximum lateral loads are 0.34% and -0.34%, correspondingly. After PN3 Specimen reached to its maximum capacity in push direction, the lateral load capacity decreased rapidly about 25% to 38 kN in the next cycle. The applied lateral load versus displacement, and the base moment-curvature curves can be seen in the Figures 3.7 and 3.8.

The mortar at the tension side of specimen during push direction cracked at 0.35% drift ratio. Early flexural cracks at the base of panels were observed at 0.35% drift ratio in mid panels. Longitudinal bars at both sides of the PN3 specimen bent at first cycle of -0.35% and second cycle of 0.35% drift ratio.

In the second cycle of the -0.5% drift ratio, under compression bottom corner of the AAC wall crushed and flexural cracks between the loading beam and panels were observed. After 1.5% drift ratio, the cracks between the panels widened, and bottom and top sections of the AAC panels cracked, and started to separate from the concrete beams. In the Figure 3.9, some pictures of the above mentioned damages are illustrated.

3.1.4 Specimen 4, PN4

The forth specimen, PN4, test was carried out with four vertical wall panels and with axial load as explained in section 2.1.6. In this section the PN4 specimen test results are presented.

In the forward and backward directions, the maximum load capacities of the specimen were 90.9 kN and -82.4 kN, respectively. These capacities were attained in the first cycle of 0.98% and -1.48% drift ratios, correspondingly. At 2.0% drift ratio, the specimen capacity reduced to 72.0 kN which was 20% of the maximum

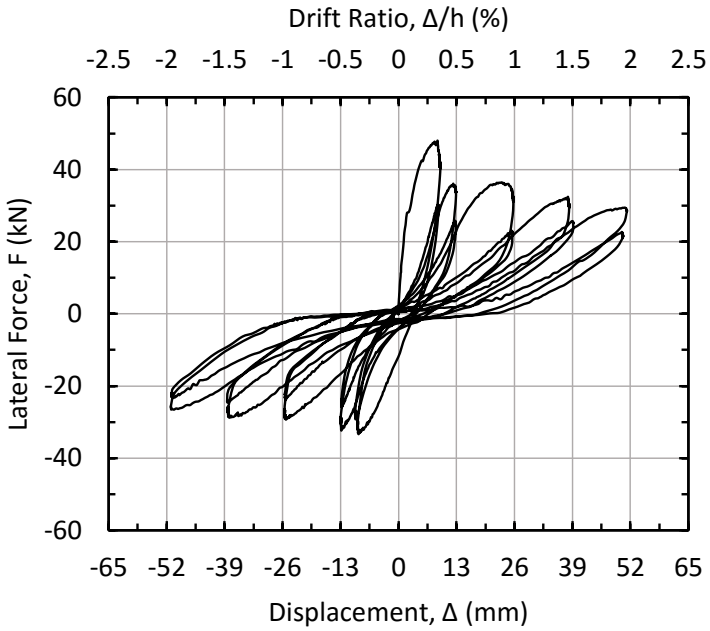

Figure 3.7: Specimen PN3 lateral load versus displacement and drift ratio

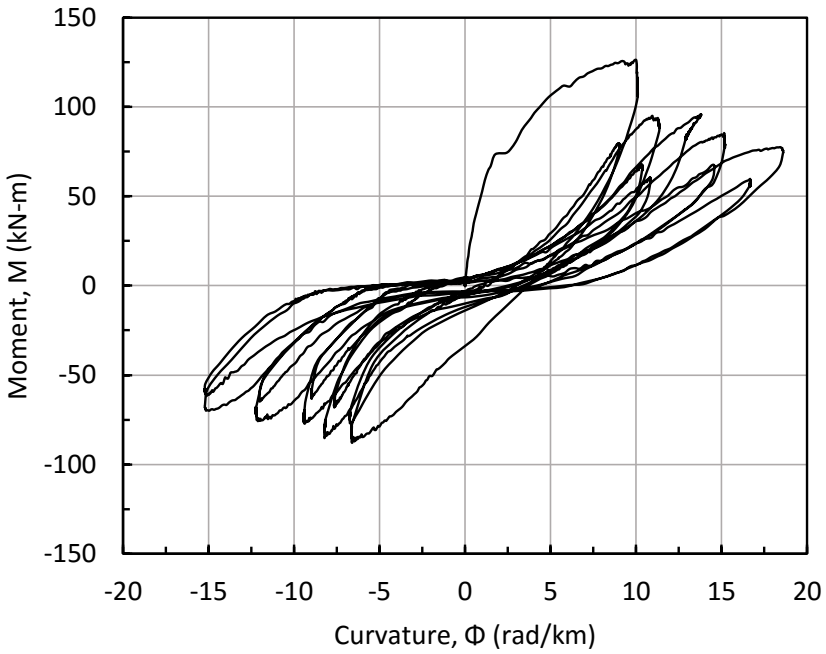

Figure 3.8: Specimen PN3 base moment-curvature

Figure 3.9: Specimen PN3 failure pictures

Figure 3.9: Specimen PN3 failure pictures (cont.)

capacity of the PN4 specimen. The applied lateral load versus displacement, and the base moment-curvature curves can be seen in the Figures 3.10 and 3.11.

The cement mortar at both sides of the PN4 specimen cracked, and the longitudinal bars bent at ±0.35% drift ratios. Early cracks at the bottom corner were observed at first cycle of 0.5% drift ratio. Both ends of the panels started to crush at ±1% drift ratio. In the first cycle of the 1.5% drift ratio, at the bottom of the panels, the cover crushed and reinforcing mesh inside the AAC panels was visible. At the end of the test, the main cracks between the AAC wall panels widened, bottom and top of the panels completely cracked, and bottom of the panels was damaged significantly. Figure 3.12, shows some failure pictures of the Specimen PN4.

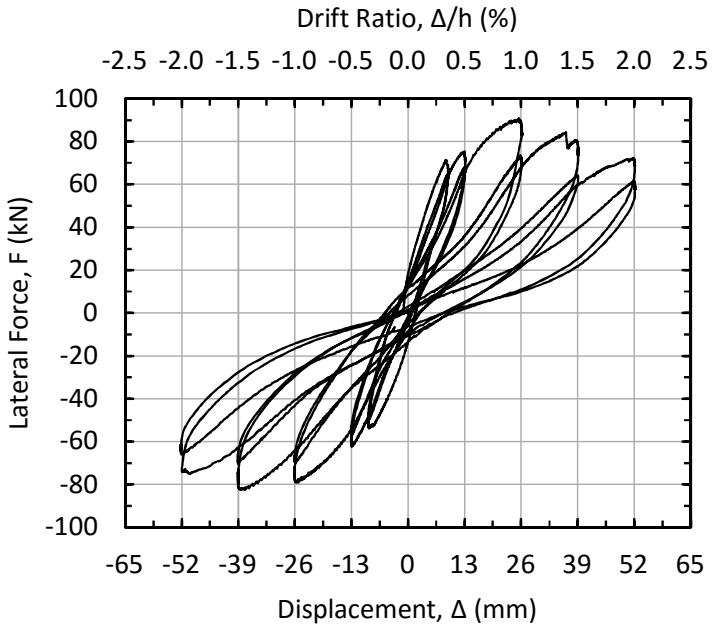

Figure 3.10: Specimen PN4 lateral load versus displacement and drift ratio

3.1.5 Specimen 5, PN5

Specimen 5 test was carried out with six vertical AAC wall panels, without axial load, and without opening as explained in section 2.1.7.

The maximum lateral load capacities of the specimen were 142.8 kN and -95 kN

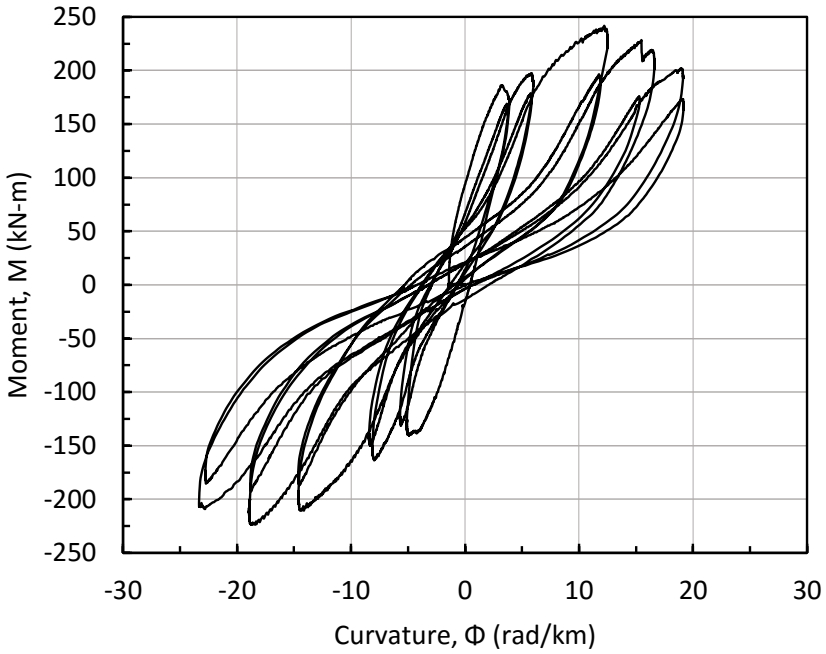

Figure 3.11: Specimen PN4 base moment-curvature

in the forward and backward directions, respectively. At the first cycle of 0.97% and -1.83% drift ratios, the maximum capacities of the specimen were attained, correspondingly. At the 1.81% drift ratio, the specimen capacity reduced to 114.2 kN which was 20% of maximum capacity of the PN5 specimen. Figures 3.13 and 3.14 show the applied lateral load versus displacement, and the base moment-curvature curves.

At the first cycle of 0.35% drift ratio, bottom corner of the panel at tension side of the specimen cracked. The ratio of length to width at bottom section of the PN5 specimen was excessive, and in every cycle it slipped instead of rotation as can be seen in Figure 3.13. In the second cycle of 0.5% drift ratio both corners of the PN5 specimen crushed. At $\pm 1\%$ drift ratio, the longitudinal bars bent and a significant crack occurred at the tension bottom corner of the outer panel. At higher drift ratios, bottom corners of the outer panels along with adjacent panels crushed. In Figure 3.15 some of the failure pictures of the PN5 specimen are illustrated.

Figure 3.12: Specimen PN4 failure pictures

Figure 3.12: Specimen PN4 failure pictures (cont.)

Figure 3.12: Specimen PN4 failure pictures (cont.)

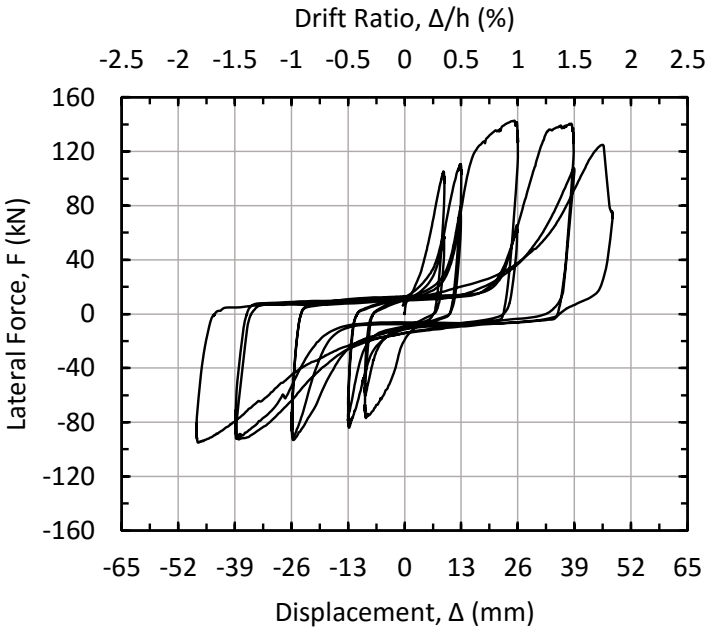

Figure 3.13: Specimen PN5 lateral load versus displacement and drift ratio

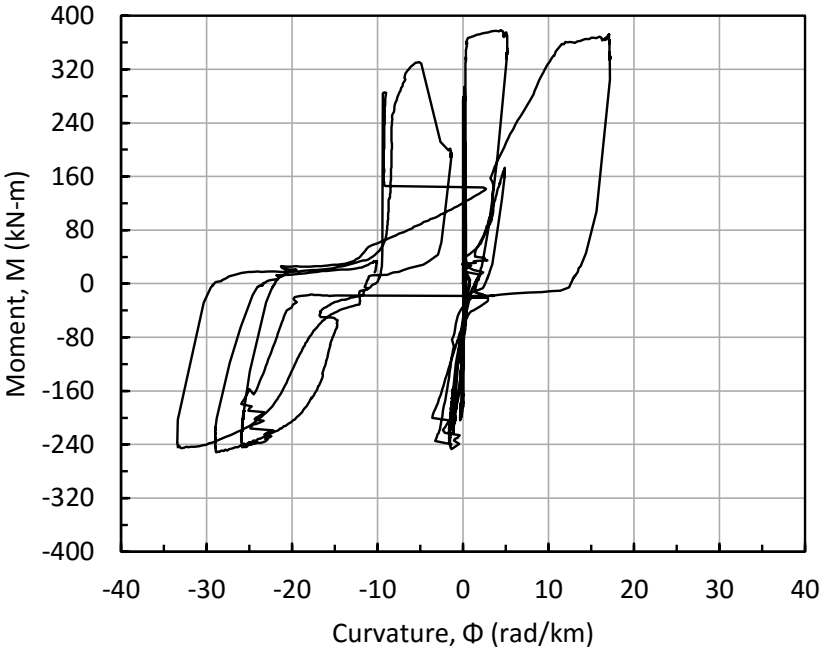

Figure 3.14: Specimen PN5 base moment-curvature

Figure 3.15: Specimen PN5 failure pictures

Figure 3.15: Specimen PN5 failure pictures (cont.)

Figure 3.15: Specimen PN5 failure pictures (cont.)

3.1.6 Specimen 6, PN6

In this section, the PN6 specimen test results are presented. As explained in section 2.1.8, PN6 test was carried out with six vertical panels, without axial load, and a 1.2 m × 1.2 m square window opening in the middle of the wall.

The maximum forward and backward loads applied to the specimen were 79.5 kN and -91.9 kN, respectively. The drift ratios corresponding to the maximum lateral loads were 0.33% and -0.97%, correspondingly. After PN6 Specimen reached to its maximum capacity in push direction, the lateral load capacity was reduced promptly about 35% to 51.38 kN in the next cycle. The applied lateral load versus displacement, and the base moment-curvature curves can be seen in the Figures 3.16 and 3.17.

At first cycle of 0.35% drift ratio, early cracks were observed at the top of the first panel and shorter wall panels under the window opening. In ±0.35% drift ratios, both joint cracks at sides of shorter wall panels widened. The cement mortar and a part of the AAC panel at the bottom compression corner of the specimen crushed in the second cycle of 0.35% drift ratio. Longitudinal bar at the compression side of the specimen bent at second cycle of 1%. Both ends of the outer panel at tension side of the specimen cracked critically in -1.5% drift ratio, and started to separate from the concrete beams. The joint cracks of the shorter panels widened until the end of the test and both steel brackets deformed. At the end of the test, cracks between the units of the outer panels widened significantly. In the Figure 3.18, flexural pictures of the PN6 specimen are presented.

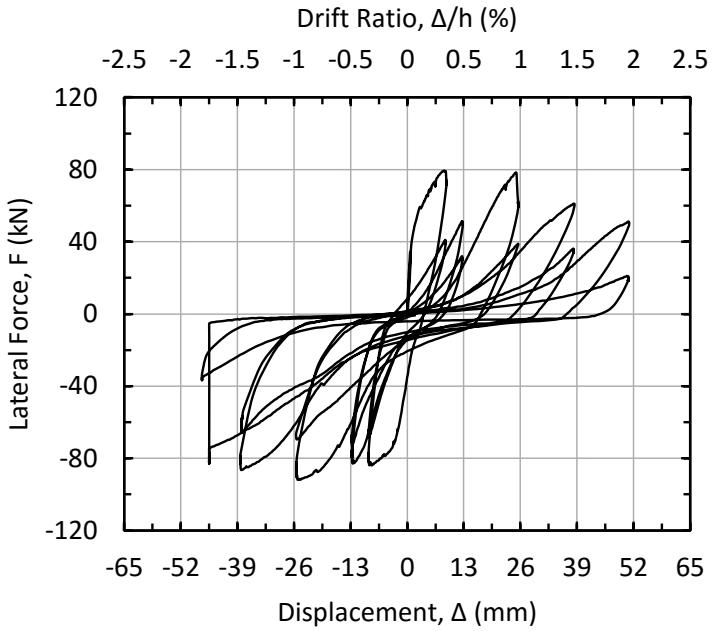

Figure 3.16: Specimen PN6 lateral load versus displacement and drift ratio

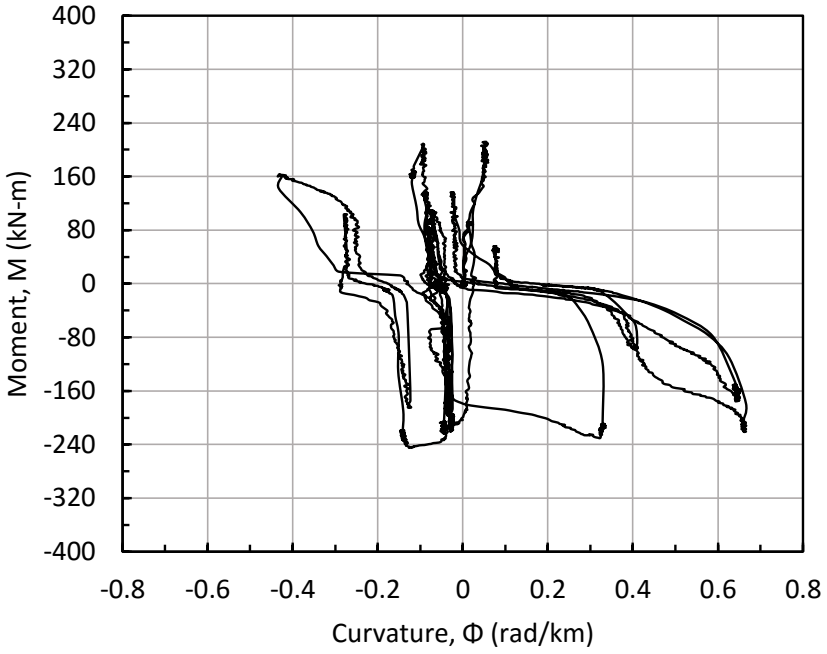

Figure 3.17: Specimen PN6 base moment-curvature

Figure 3.18: Specimen PN6 failure pictures

Figure 3.18: Specimen PN6 failure pictures (cont.)

Figure 3.18: Specimen PN6 failure pictures (cont.)

CHAPTER 4

EVALUATION OF TEST RESULTS

4.1 Discussion of Test Results

Test results of all specimens will be critically discussed in this section. In Figures 4.1 and 4.2, load-displacement backbone curves of specimens with 2 and 4 panels are presented. To obtain the backbone curves, the peak points of each cycles were selected in both positive and negative directions.

Figure 4.1 and 4.2 clearly indicates that lateral load capacity of Specimen PN2 with axial load is almost three times greater than PN1 Specimen without axial load, and similarly lateral load capacity of Specimen PN4 with axial load is two times greater than Specimen PN3 without axial load.

Figure 4.3 shows all curves on the same graph. As can be seen from the figure, as the number of panels increases, consequently lateral load capacity increases almost linearly.

From Figure 4.4, it can be concluded that specimens PN1 and PN3 (without axial load) reached to the maximum capacity at lower drift ratios (0.35%), whereas in specimens PN2 and PN4 (with axial load), the peak point of the curves are reached at higher drift ratios (1%). In opposition to this observation, the expected behavior should be a reduction in drift under axial load. Most probably, axial load helps to keep vertical panels together and thus increases the drift. Values in Table 4.1 were deducted from the backbone curves of the specimen.

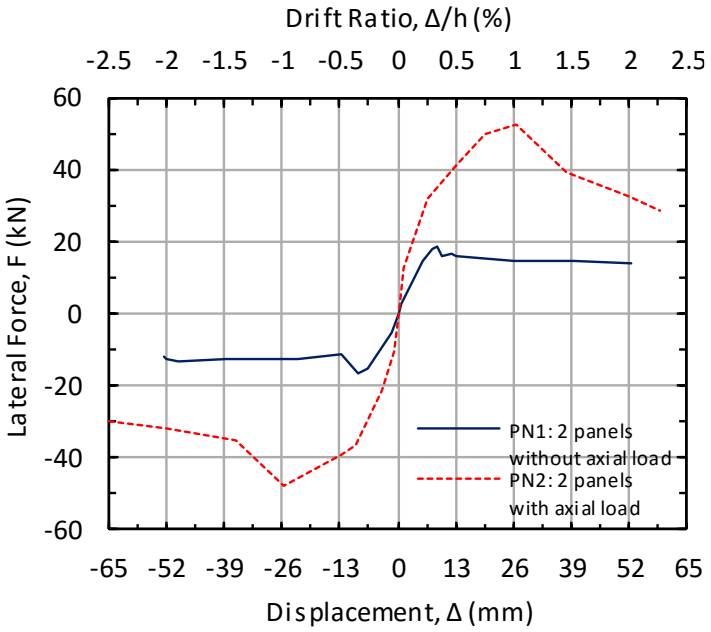

Figure 4.1: Specimens PN1 amd PN2 backbone curves

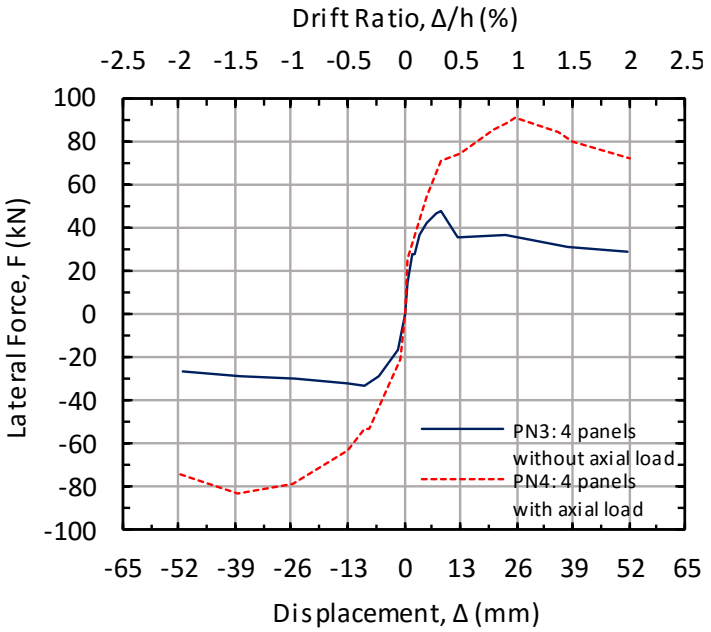

Figure 4.2: Specimens PN3 amd PN4 backbone curves

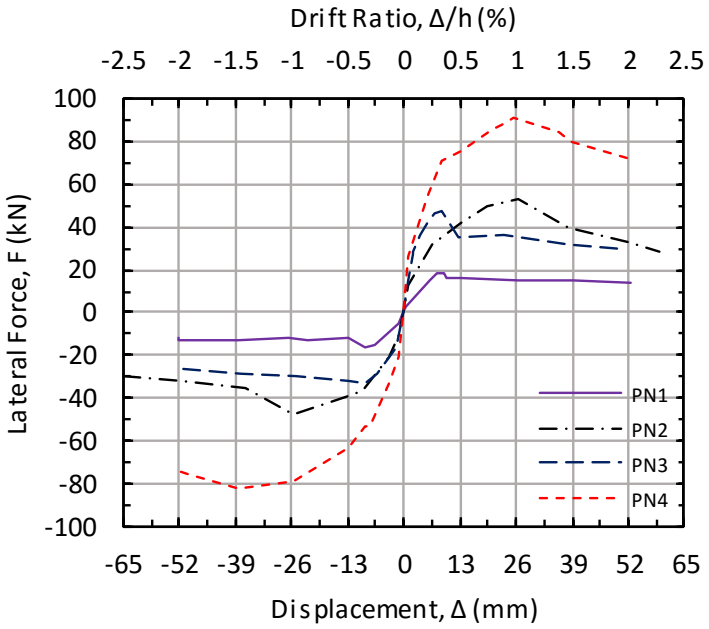

Figure 4.3: Specimens PN1, PN2, PN3 amd PN4 backbone curves

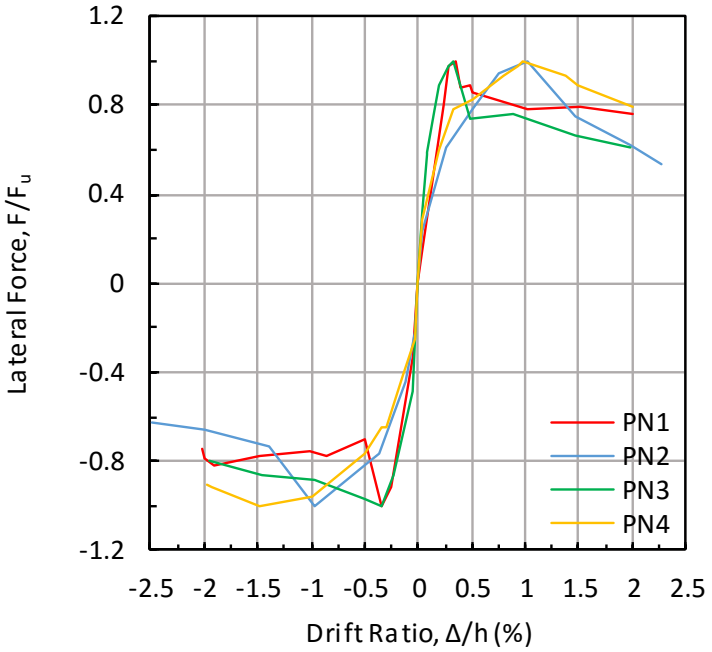

Figure 4.4: Specimens PN1, PN2, PN3 amd PN4 normalized backbone curves

4.2 Ductility

Assuming equal energy principal, equations 4.1, 4.2 and 4.3 are used to calculate displacement ductility, μ_Δ, curvature ductility, μ_ϕ, and behavior factor R_μ, of the AAC walls. For each of the specimens, from the moment-curvature and lateral load-displacement curves, corresponding values of displacement, Δ, yield lateral load, V_y, and the ultimate lateral load V_u, are obtained. In these calculations, V_u is equal to 80% of the maximum applied lateral load, V_{max}. The value of Δ_y is obtained by crossing the horizontal line passing through the maximum load and the line drawn from origin through 70% of lateral load capacity. These values are presented in Table 4.1.

$$\mu_\Delta = \frac{\Delta_u}{\Delta_y} \tag{4.1}$$

$$\mu_\phi = \frac{\phi_u}{\phi_y} \tag{4.2}$$

$$R_\mu = \sqrt{2\mu - 1} \tag{4.3}$$

The new proposed Turkish Earthquake Code (TEC 2016) gives for reinforced AAC panel buildings a value of 3 for structural behavior factor, R, and 2 for over-strength factor [TEC, 2016]. From Table 4.1, displacement ductility values, μ_Δ, for PN1 and PN3 specimens (without axial load) are 3.16 and 3.65, respectively. On the other hand, the ductility values for PN2 and PN4 specimens (with axial load) are 4.72 and 4.42, respectively. The value of R_μ which is reduction factor due to ductility, should be multiplied by over-strength factor which can be taken as approximately 1.2-1.5 to get structural system behavior factor. According to Table 4.2, all R values are higher than 3 as proposed in TEC 2016. Therefore, it can be concluded that the proposed R value of 3 in TEC 2016 is on the safe side for AAC panel wall structures.

If the drift ratios in Table 4.1 are evaluated, it can be concluded that ultimate drift ratios are greater than 1% with the exception of specimen PN1. Therefore, 1% will be proposed for ultimate drift ratio of walls composed of reinforced vertical AAC panels.

Table 4.1: Summary of test results

Test	$\mathbf{V_{cr}}$ **(kN)**	$\mathbf{V_y}$ **(kN)**	$\mathbf{V_u}$ **(kN)**	$\mathbf{V_{max}}$ **(kN)**	$\mathbf{\Delta_y}$ **(mm)**	$\mathbf{\Delta_u}$ **(mm)**	$\mathbf{\Delta_{max}}$ **(mm)**	$\boldsymbol{\mu_\Delta}$	$\boldsymbol{\phi_y}$	$\boldsymbol{\phi_u}$	$\boldsymbol{\mu_\phi}$	$\mathbf{DR_y}$ (%)	$\mathbf{DR_u}$ (%)	**Failure mode**
PN1	4.66 (-5.4)	16.4 (-14.9)	15.0 (-13.0)	18.7 (-16.2)	6.7 (-6.7)	21.2 (-20.5)	8.97 (-9.1)	3.16 (-3.1)	5.4 (-5.7)	16.9 (-18.6)	3.13 (3.25)	0.26 (-0.26)	0.82 (-0.79)	Flexural
PN2	13.2 (-11.9)	32.8 (-35.9)	42.4 (-38.3)	53.0 (-47.9)	7.15 (-9.2)	33.8 (-33.3)	25.4 (-25.4)	4.72 (-3.6)	N.A.	N.A.	N.A.	0.28 (-0.35)	1.3 (-1.28)	Flexural
PN3	24.5 (-16.3)	36.7 (-28.7)	35.9 (-26.7)	48.0 (-33.4)	6.5 (-6.0)	23.7 (-50.2)	8.89 (-9.1)	3.65 (-8.4)	5.4 (-5.2)	11.2 (-12.0)	2.10 (2.31)	0.25 (-0.23)	0.91 (-1.93)	Sliding, Flexural
PN4	15.9 (-19.6)	73.7 (-69.4)	72.7 (-65.9)	90.9 (-82.4)	11.7 (-17.3)	51.7 (-52.0)	25.3 (-39.0)	4.42 (-3.0)	4.8 (9.5)	20.6 (-23.2)	5.15 (2.44)	0.46 (-0.66)	1.99 (-2.00)	Flexural
PN5	14.8 (-33.5)	110.6 (-78.2)	114.2 (-76.0)	142.8 (-95.0)	12.8 (-9.9)	47.0 (-47.5)	25.2 (-25.6)	3.67 (-4.8)	N.A.	N.A.	N.A.	0.49 (-0.38)	1.81 (-1.83)	Sliding
PN6	38.9 (-19.2)	68.4 (-76.3)	63.6 (-73.5)	79.5 (-91.9)	5.18 (-4.9)	37.2 (-46.2)	9.02 (-25.5)	7.18 (-9.5)	N.A.	N.A.	N.A.	0.13 (-0.18)	1.43 (-1.78)	Sliding

Table 4.2: Structure system behavior factor, R

Specimen	$\mathbf{R_\mu}$	$\mathbf{1.2R_\mu}$	$\mathbf{1.5R_\mu}$
PN1	2.31	2.77	3.46
PN2	2.91	3.49	4.36
PN3	2.51	3.01	3.76
PN4	2.80	3.36	4.20
PN5	2.52	3.02	3.78
PN6	3.66	4.39	5.48

4.3 Failure Mode

From the load-displacement curves and observations during the tests, either flexural, shear, or interface shear failure mode was selected as the dominated failure mode. Moreover, in some of the tests separation of vertical panels were seen. Furthermore, according to the Table 4.6, the least calculated value among V_{shear}, $V_{diagonal}$ and $V_{flexure}$ can indicate the dominated failure mode.

4.4 Moment-Curvature Analysis

To obtain analytical moment-curvature curves, section analysis for each specimen have been conducted by RESPONSE2000 software. Steel properties obtained from coupon tests were used in the analytical calculations. In the figures below, the analytical results and results obtained from the experiments are compared.

4.4.1 Specimen PN1

The moment-curvature analysis has been done for specimen PN1 with 2 vertical AAC panels and 1.2 m $\times$ 0.2 m plan area. This specimen has 3 longitudinal bars. No axial load was applied to this specimen. The ultimate strength is predicted in both directions acceptably well. At high displacement demands,

the behavior is overestimated by the analysis. This difference can be attributed to the early buckling of longitudinal bars under compression at both ends due to the mortar spalling in half grooves and lost of bond.

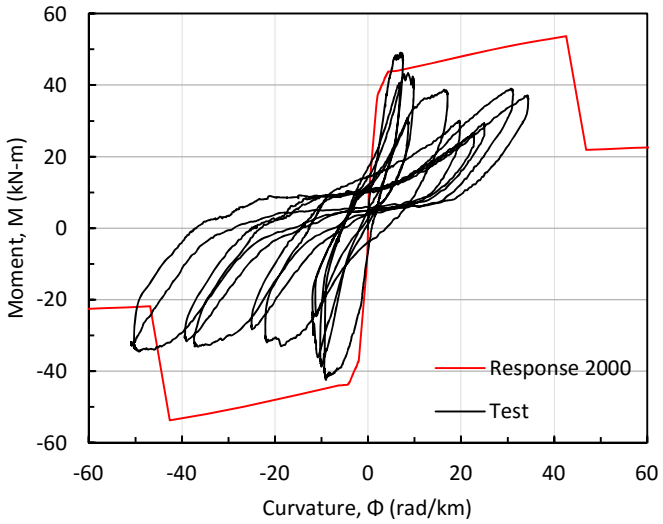

Figure 4.5: Specimen PN1 experimental vs analytical moment-curvature

4.4.2 Specimen PN2

Specimen PN2 is the same specimen with PN1 with the exception of axial load application during test. The ultimate strength is also reasonably predicted in this specimen.

4.4.3 Specimen PN3

This specimen was constructed with 4 vertical AAC panels, and therefore had 5 longitudinal bars. The test was conducted under no axial load. Again, spalling mortar around bars at both ends of the wall and buckling was the main problem for this specimen. The strength prediction in the positive direction is satisfactory.

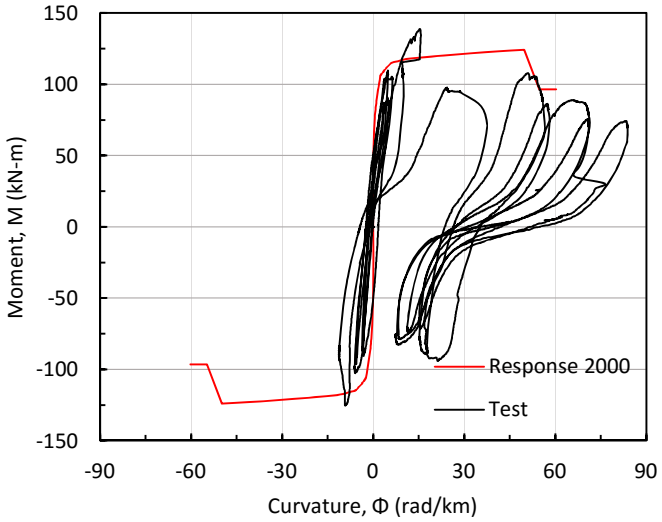

Figure 4.6: Specimen PN2 experimental vs analytical moment-curvature

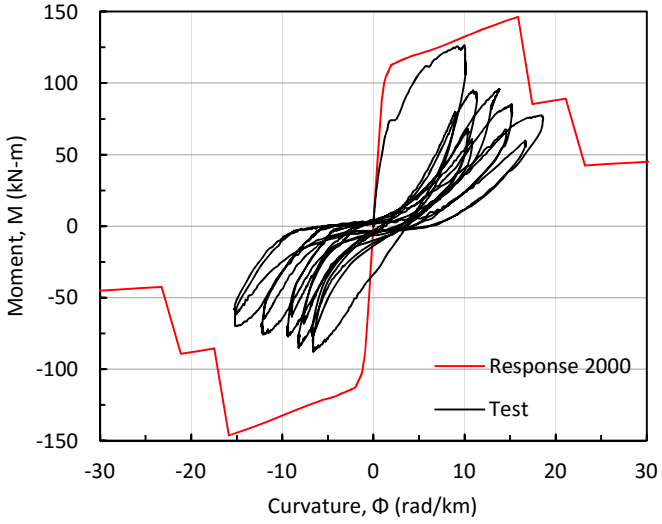

Figure 4.7: Specimen PN3 experimental vs analytical moment-curvature

4.4.4 Specimen PN4

Specimen PN4 is the very same specimen with PN3 with the only difference of inclusion of axial load during testing. Analytical curve given in Figure 4.8 is in good agreement with the experimental results. The prediction of this specimen is better than specimen PN3 because of positive impact of axial load on panels as monolithic units.

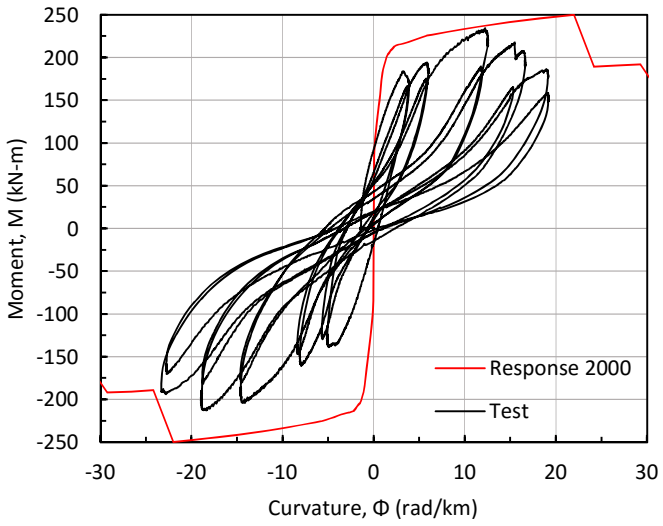

Figure 4.8: Specimen PN4 experimental vs analytical moment-curvature

4.4.5 Specimens PN5 and PN6

The last two tests, PN5 and PN6, were conducted with 6 panels. Panel separation and rocking was excessive in these tests. Therefore, curvature measurements were not reliable in these tests. Figure 4.9 shows M-ϕ curve for specimen PN5. As can be seen in the figure, there are unexpected slip in the curve. PN6 curve is totally ignorable.

4.5 Moment-Axial Load Interaction Analysis

The moment-axial load interaction analysis of specimens have been conducted by RESPONSE2000 software. In the figures below, the experimental tests data

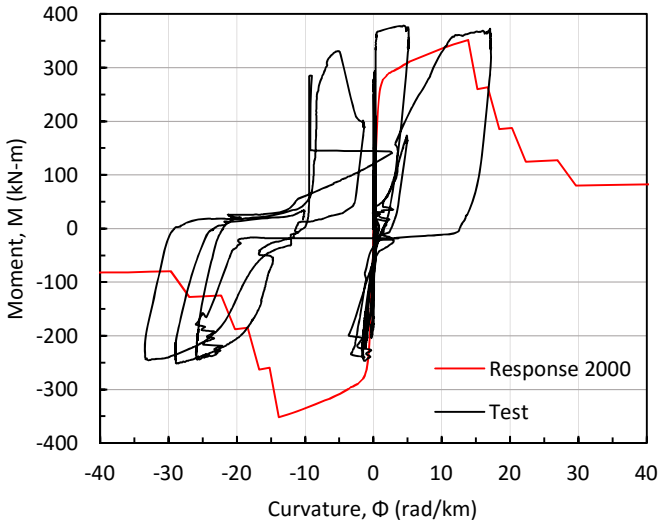

Figure 4.9: Specimen PN5 experimental vs analytical moment-curvature

and analytical results are compared. The solid M-N curve was calculated by considering yield strength of longitudinal bars, whereas in dashed M-N curve, strain hardening of steel was taken into account. Figure 4.10 shows that the analytic M-N curve fits to the experimental data quite good. It can be concluded that wall units composed of 2 vertical AAC panels function as monolithic walls. The experimental data for maximum moment and corresponding axial load couple for each specimen are presented in Table 4.3.

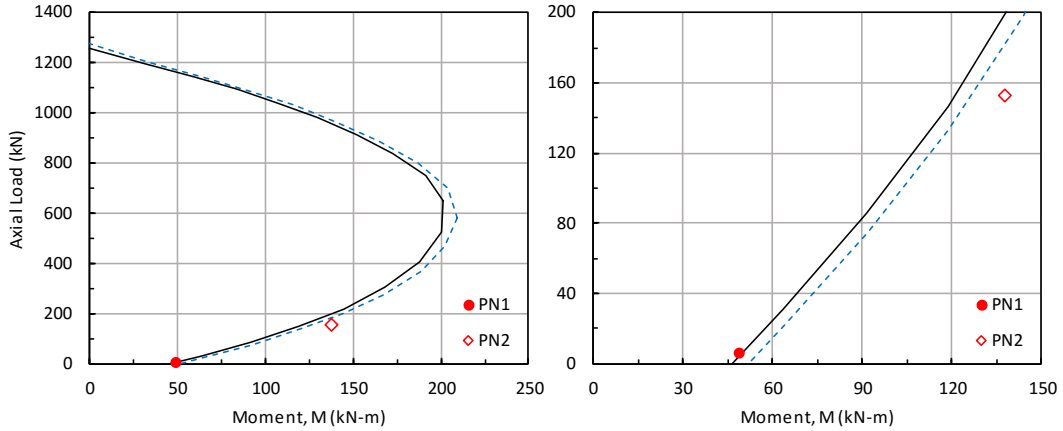

Figure 4.10: M-N interaction diagram for specimens PN1 and PN2

Figure 4.11 compares the results of walls made of 4 panels. Analytical M-N curve acceptably matches experimental data points. The divergence of data

point with axial load may be explained by not functioning the 4 panels as a monolithic wall.

Figure 4.12 shows the results for Specimen PN5 and PN6. According to the figure, capacity is overestimated analytically. The reason can be attributed to the window opening in this specimen which surely decreased the capacity and altered the behavior.

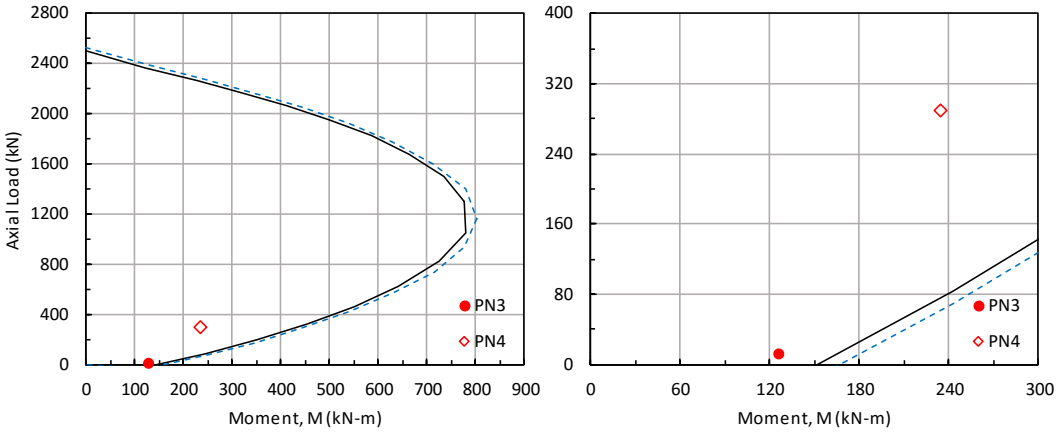

Figure 4.11: M-N interaction diagram for specimens PN3 and PN4

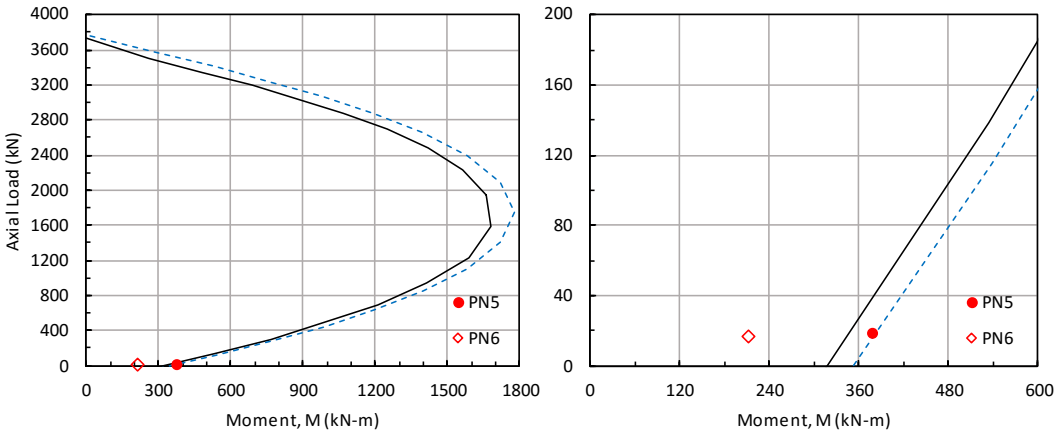

Figure 4.12: M-N interaction diagram for specimens PN5 and PN6

4.6 Deformation Components

By using the equations 4.4 and 4.5, the experimental data of each test is evaluated and deformation components of tests are separated to slip, Δ_{slip}, flexural

Table 4.3: Maximum moment and corresponding axial load for each specimen

Specimen	**N (kN)**	**M (kN-m)**
PN1	6.2	49.0
PN2	152.3	137.7
PN3	12.4	126.5
PN4	289.5	236.3
PN5	18.7	378.4
PN6	16.7	211.8

deformation which contains elastic, $\Delta_{elastic}$, and inelastic parts, $\Delta_{inelastic}$, and shear deformation, Δ_{shear}.

$$\begin{aligned}\Delta_t &= \Delta_{slip} + \Delta_{flexural} + \Delta_{shear} \\ &= \Delta_{slip} + \Delta_{elastic} + \Delta_{inelastic} + \Delta_{shear} \\ &= \Delta_{slip} + \frac{\phi_y L^2}{3} + (\phi_u - \phi_y) L_p L + \frac{VL}{GA_s} \end{aligned} \tag{4.4}$$

$$A_s = \frac{5}{6} A_g \tag{4.5}$$

where:

ϕ_y = the value of curvature in the yield point from moment-curvature graph, rad/mm

ϕ_u = the value of curvature in the desired drift ratio point from moment-curvature graph, rad/mm

A_s = shear area of the specimen, mm^2

A_g = gross area of the specimen, mm^2

G = shear modulus of material, MPa

L = the height of the specimen, mm

L_p = the plastic length of the specimen, mm

V = applied lateral load, N

The deformation components of the PN1, PN3 and PN4 specimens at 1% drift

ratio are presented in Figure 4.13. As the specimens PN2, PN5 and PN6 moment-curvature curves are not sufficient enough to obtain the desirable parameters, the results of these specimens are not given in this dissertation. Table 4.4, represents the values of parameters L, L_p, A_s and G for the specimens. Furthermore, in the Table 4.5, the participation of each factor in deformation are presented.

Table 4.4: Parameters for specimens PN1, PN3 and PN4

Specimen	**L (mm)**	**L_p (mm)**	**A_s (mm^2)**	**G (MPa)**
PN1	2600	500	200,000	1042
PN3	2600	800	400,000	1042
PN4	2600	800	400,000	1042

Table 4.5: Deformation component for specimens PN1, PN3 and PN4

Components	**PN1**	**PN3**	**PN4**
Δ_{test} (mm)	26.45	26.20	25.93
Δ_{slip} (mm)	4.90	1.31	1.61
$\Delta_{elastic}$ (mm)	12.17	12.17	10.82
$\Delta_{inelastic}$ (mm)	15.18	15.66	19.05
Δ_{shear} (mm)	0.18	0.20	0.54
Total (mm)	32.43	29.33	32.02
Unaccounted (mm)	5.98	3.13	6.09

By comparing the results in Figure 4.13, different deformation components can be obtained. In PN1 specimen there was no axial load and hence, sliding is more than that of the other specimens. Flexural deformation which contains the elastic and inelastic parts was the most dominated part in all of the specimens. It is clear that the shear component dominated more as the specimens dimensions get bigger and the axial load increased. The unaccounted part is the difference between the experimental data and the analytical calculations. Most of the error is probably because of the relative vertical sliding between the AAC panels.

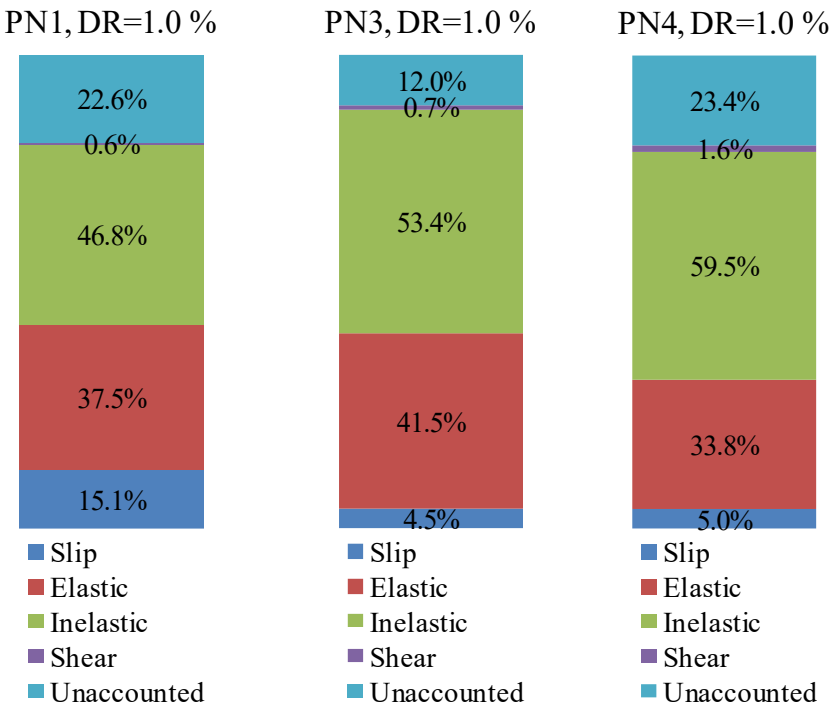

Figure 4.13: Specimens PN1, PN3 and PN4 deformation components

4.7 Energy Dissipation

To obtain the energy dissipated in each cycle of the tests, the area under the load-displacement curves are calculated. Figure 4.14 shows the dissipated energy of every cycle. The second cycle of every drift ratio dissipates less energy as compared to the first cycle of that drift level. The main reason for this decrease can be attributed to the strength degradation at the second cycle. On the same graph, the cumulative dissipated hysteretic energies are also included.

In Figure 4.15, all cumulative energies are shown on the same figure for comparison purposes. It can be concluded that as panel number increases the dissipated cumulative energy increases. Additionally, for the same number of panels, inclusion of axial load also increases the cumulative energy. The window opening in specimen PN6 caused a decrease in the cumulative energy as expected.

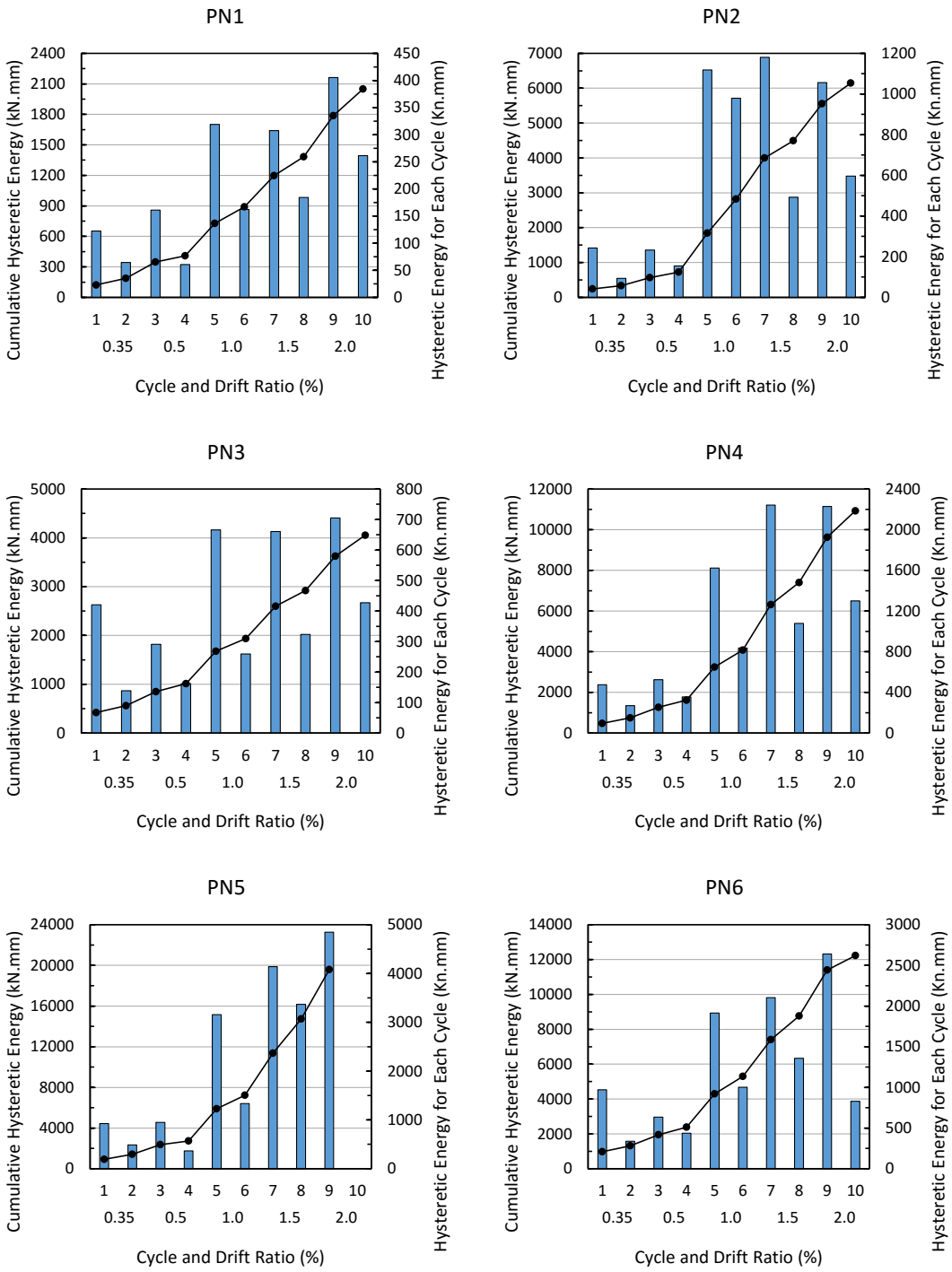

Figure 4.14: Dissipated energy in all specimens

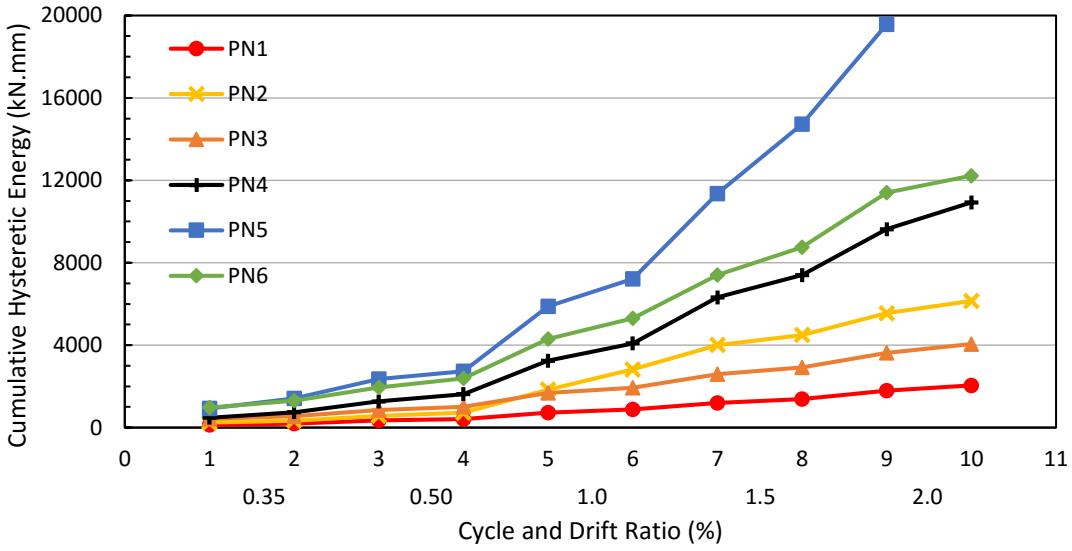

Figure 4.15: Cumulative dissipated energy in all specimens

4.8 Nominal Strength

4.8.1 According to Building Code Requirements for Masonry Structures (MSJC 2011)

According to Building Code Requirements for Masonry Structures (TMS 402/ ACI 530/ASCE 5) [MSJC, 2011], Nominal shear strength, V_n, shall be computed using equation 4.6:

$$V_n = V_{nAAC} + V_{ns} \tag{4.6}$$

where V_n shall not exceed the following:

$$V_n = \mu_{AAC} P_u \tag{4.7}$$

where μ_{AAC} is the coefficient of friction and equals to 0.75 between AAC and AAC, and shall be 1.0 between AAC and thin-bed mortar or between AAC and leveling-bed mortar.

For $M_u/(V_u d_v) \geq 1.0$

$$V_n \leq 0.33 A_n \sqrt{f'_{AAC}} \tag{4.8}$$

The nominal masonry shear strength shall be taken as the least of the values

governed by web-shear cracking and crushing of diagonal compressive strut computed by equations 4.9 or 4.10, and 4.11.

The Nominal shear strength as governed by web-shear cracking, V_{nAAC}, shall be computed using equations 4.9 for AAC masonry with mortared head joints, and equation 4.10 for masonry with unmortared head joints.

$$V_{nAAC} = 0.08 l_w t \sqrt{f'_{AAC}} \sqrt{1 + \frac{P_u}{0.2\sqrt{f'_{AAC}} l_w t}} \quad \text{(mortared head joints)} \tag{4.9}$$

$$V_{nAAC} = 0.055 l_w t \sqrt{f'_{AAC}} \sqrt{1 + \frac{P_u}{0.2\sqrt{f'_{AAC}} l_w t}} \quad \text{(unmortared head joints)} \tag{4.10}$$

For walls with $M_u/(V_u d_v) < 1.5$, nominal shear strength, V_{nAAC}, as governed by crushing of diagonal compressive strut, shall be computed by equation 4.11:

$$V_{nAAC} = 170,000 f'_{AAC} t \left[\frac{h(l_w)^2}{h^2 + \left(\frac{3l_w}{4}\right)^2} \right] \tag{4.11}$$

The parameters in the equations above, are as below:

A_n = net cross-sectional area of a member, mm^2

d_v = actual depth of a member in direction of shear considered, mm

f'_{AAC} = specified compressive strength of AAC masonry, MPa

h = effective height of column, wall, or pilaster, mm

l_w = length of entire wall or of the segment of wall considered in direction of shear force, mm

M_u = factored moment, $N - mm$

P_u = factored axial load, N

t = nominal thickness of member, mm

V_{nAAC} = nominal shear strength provided by AAC masonry, N

V_{ns} = nominal shear strength provided by shear reinforcement, N

V_u = factored shear force, N

In Table 4.6, the minimum of V_{shear}, $V_{diagonal}$ and $V_{flexure}$ should be compared with test results and taken as failure load. In Specimen PN1, analytical calculations addresses flexural failure which was also observed during the test. The difference between the calculated and measured lateral load was only 4.8% but on the unsafe side. In Specimen PN2, the lateral load capacity was much higher as compared to Specimen PN1 due to the presence of axial load during test. Both the calculated and observed failure mode was flexure in this specimen. The calculated value underestimated the test value by 19.8%. For Specimens PN3 and PN4, calculations refer to shear failure. However, observations showed sliding and flexural failure. The reason can be the smooth base without any leveling mortar which eases sliding and therefore prevents shear failure. The error between the calculated and measured values were 20.8% and 6.2% for PN3 and PN4, respectively. Similar to 2 panel case, exclusion of axial load in specimen with 4 panels caused unsafe prediction by MSJC 2011. For Specimen PN5 with 6 panels and excluding axial load, the failure prediction was unacceptably high. The shear capacity is predicted very low. However, flexural failure was observed during the test. If flexural capacity is compared with test result, the error is only 4.5% and also on the safe side. It is believed that due to the window opening and panel arrangement, it is not meaningful to compare the calculated and measured values for Specimen PN6. May be this specimen should be considered as 1+3 panel configuration.

Table 4.6: Results based on Building Code Requirements for Masonry Structures (MSJC 2011)

Test	$\mathbf{V_{shear}}$ **(kN)**	$\mathbf{V_{diagonal}}$ **(kN)**	$\mathbf{V_{flexure}}$ **(kN)**	$\mathbf{V_{test}}$ **(kN)**	**Difference (%)**	$\mathbf{V_{n1}}$ **(kN)**	$\mathbf{V_{n2}}$ **(kN)**
PN1	29.2	67.3	19.6	18.7	4.8	120	158.4
PN2	42.6	67.3	42.5	53.0	-19.8	120	158.4
PN3	58	203.7	64.2	48.0	20.8	240	316.8
PN4	85.3	203.7	155.5	90.9	-6.2	240	316.8
PN5	87.6	326.2	136.4	142.8	-36.5	360	475.2
PN6	87.6	326.2	136.4	79.5	10.2	360	475.2

4.8.2 According to Draft Turkish Earthquake Code 2016 (TEC 2016)

According to the new proposed Turkish Earthquake Code 2016 [TEC, 2016], the equations 4.12, 4.13, and 4.14 are proposed to calculate the lateral capacity of the reinforced AAC panel walls. The minimum value obtained from the equations is the capacity of the wall.

$$V_{Rd1} = 0.15lt\sqrt{f_d} \tag{4.12}$$

$$V_{Rd2} = N_{Ed} + 0.3\Sigma A_{si} f_{yd} \tag{4.13}$$

$$V_{Rd3} = 0.2lt f_d \tag{4.14}$$

where:

A_{si} = longitudinal bars area in reinforced panel walls , mm^2

f_d = specified compressive strength of panels, MPa

l = length of wall, mm

N_{Ed} = applied axial load, N

t = nominal thickness of wall, mm

V_{Rd} = nominal lateral load capacity of panel walls, N

The results obtained using the equations of TEC 2016 are presented in Table 4.7. First, in order to compare the effect of number of panel without considering axial load, specimens PN1, PN3, and PN5 will be discussed. While the proposed equations overestimate to be on the unsafe side the capacity for 2 panels, the capacities are underestimated with an increasing error for 4 and 6 panels, respectively. The errors for 2, 4 and 6 panels are 33.2%, -9.2%, and -56.4%, respectively.

To evaluate the effect of axial load, specimens PN2 and PN4 should be considered. For both cases, capacities are overestimated which means unsafe prediction. The error increases as the number of panel increases. While the error is 35.8% for 2 panel, it increases to 58.4% for 4 panels.

Table 4.7: Results based on Turkish Earthquake Code 2016 (TEC 2016)

Test	$\mathbf{V_{Rd1}}$ **(kN)**	$\mathbf{V_{Rd2}}$ **(kN)**	$\mathbf{V_{Rd3}}$ **(kN)**	$\mathbf{V_{Rd}}$ **(kN)**	$\mathbf{V_{test}}$ **(kN)**	**Difference (%)**
PN1	72	24.9	192	24.9	18.7	33.2
PN2	72	144.9	192	72	53.0	35.8
PN3	144	43.6	384	43.6	48.0	-9.2
PN4	144	283.6	384	144	90.9	58.4
PN5	216	62.2	576	62.2	142.8	-56.4
PN6	216	60.2	576	60.2	79.5	-24.3

4.9 Estimation with Different Number of Panels

During the tests of some specimens, vertical joints between the panels widened and it probably affected the capacity of the specimens. In this section, the capacity of specimens PN3, PN4 and PN5 are evaluated by means of the method explained below.

The moment-axial load interaction diagrams have been obtained by RESPONSE 2000 for samples with 1, 2, 3 and 4 AAC panels to calculate the flexural capacities. The calculated moment values divided by the height of the tested specimens (2.6 m) give the base shears of theoretical samples. Moreover, for specimens PN3, PN4 and PN5, a monolithic behavior is assumed and flexural capacities are calculated. Furthermore, according to MSJC 2011, the web shear capacities of the samples for single panel and monolithic walls have been obtained by equation 4.10. In Figures 4.16 and 4.17, the aforementioned curves, and data point of specimens are presented.

From the figures, it can be observed that PN3 and PN4 specimens with 4 vertical panels did not behave as a monolithic wall and it can be recommended to calculate the flexural capacity of 4 panels as the summation of 2 groups composed of 2 panels. On the other hand, the test capacity value of PN5 specimen with 6 vertical panels is close to the flexural capacity as a monolithic wall. The PN6 specimen which had window opening, behaves as groups in 4 and 2 panels.

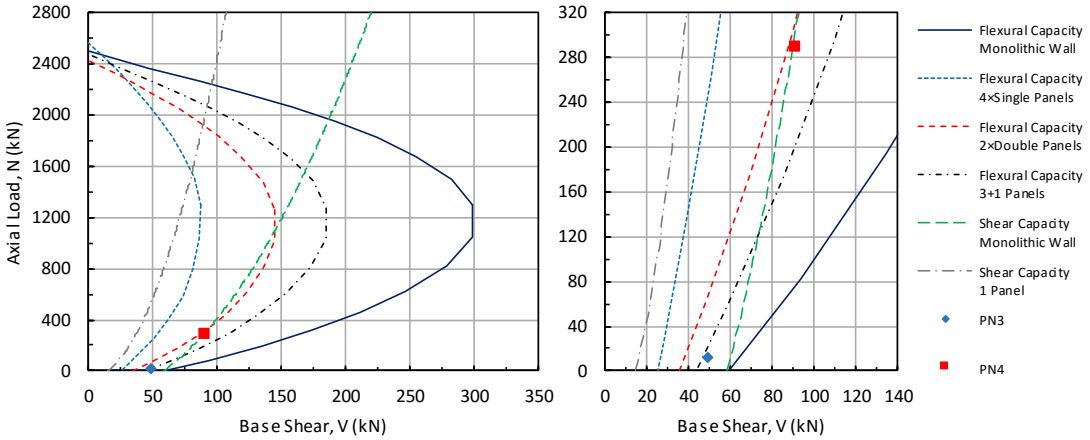

Figure 4.16: Capacity of PN3 and PN4 specimens considering different number of panels

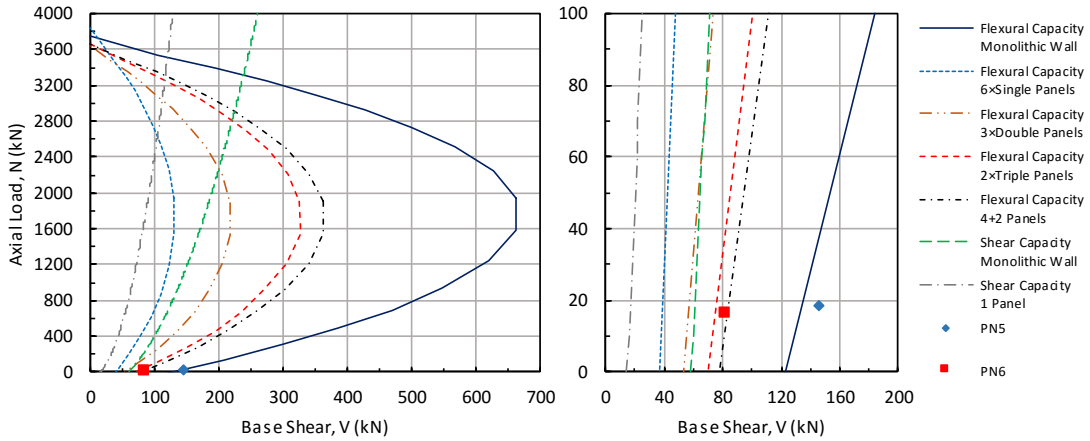

Figure 4.17: Capacity of PN5 and PN6 specimens considering different number of panels

CHAPTER 5

CONCLUSION

5.1 Summary

The in-plane seismic behavior of autoclaved aerated concrete (AAC) vertical load-bearing wall panels were examined in this dissertation. Because of the complex behavior of AAC shear walls under cyclic lateral loading and axial load, the design provisions are fundamentally important. To validate proposed design provisions for AAC structures in Turkey, different AAC shear wall specimens were tested. Six specimens with different properties and geometries were constructed and tested. Test samples were made of various numbers of wall panel units, laid vertically. No base leveling mortar was applied at the base of panels. Specimens with two and four vertical units were tested with and without axial load. Finally, specimens with six vertical wall panels were tested with and without window opening and excluding axial load.

The tests were done by applying cyclic lateral load. Different measuring devices like LVDTs and load cells were installed to acquire the data and perceive the behavior of the samples. The experimental results were compared to the analytical results to verify the proposed values of the codes, and to understand the behavior of panel walls composed of 2, 4, and 6 panels.

5.2 Conclusion

From the limited tests results following conclusions can be drawn:

- The value 3 for structural behavior factor, R, given in the new proposed Turkish Earthquake Code (TEC 2016) seems to be fairly acceptable and on the safe side according to the test results.
- In specimens PN1 and PN3 (without axial load) the specimen reached to its maximum capacity at lower drift ratios (0.35%), whereas in specimens PN2 and PN4 (with axial load) the peak points of the curves occurred at higher drift ratios (1%). Additionally, specimens with axial load represented more ductile behavior compared to their companion specimens.
- Ultimate drift ratio should be limited to 1%.
- Flexural and sliding were the most dominated failure modes in the experiments. Shear cracks are not observed during the experiments and web shear failure mode was never dominated. It should be noted that, base leveling mortar was not used in construction of all of the specimens.
- As can be seen in PN5 specimen, rocking is possible as the length of the AAC wall increases.
- In specimens with 4 or 6 wall panels, vertical separation of panels is possible.
- Flexural deformation was the most dominant component among the flexure, shear and sliding deformation of specimens PN1, PN3, and PN4.
- MSJC 2011 overestimates unsafely the strength of walls with 2 and 4 panels without axial load. For specimens with axial load, estimations of MSJC 2011 are on the safe side.
- TEC 2016 design provision estimated unsafely the capacities of 2 panel walls both with and without axial load.
- TEC 2016 design provision calculated the capacity of 4 panel wall with axial load unsafely.
- In order to obtain higher strength, to retard sliding, and to improve the behavior, it may be recommended to use bed/leveling mortar at the base of panels during construction.

- The use of mortar vertically between the panels may improve the behavior of the panel walls.

REFERENCES

[Al-Shaleh and Attiogbe, 1997] Al-Shaleh, M. and Attiogbe, E. K. (1997). Flexural strength characteristics of non-load bearing masonry walls in Kuwait. *Materials and Structures*, 30(5):277–283.

[Argudo, 2003] Argudo, J. F. (2003). *Evaluation and Synthesis of Experimental Data for Autoclaved Aerated Concrete*. PhD thesis, The University of Texas at Austin.

[Brightman, 2000] Brightman, M. J. (2000). *AAC Shear Wall Specimens: Development of Test Setup and Preliminary Results*. PhD thesis, The University of Texas at Austin.

[Building Research Institute (NISI), 1997] Building Research Institute (NISI) (1997). Carrying out Experimental Investigations to Determine the Behavior and the Bearing Capacity of Autoclaved Concrete Walls with Confining Reinforced Concrete Elements under Reversible Horizontal Load. Technical report, Building Research Institute NISI, Sofia, Bulgaria.

[Chusid, 1999] Chusid, M. (1999). Building with autoclaved aerated concrete. In *Masonry Construction, January*, pages 24–27.

[Costa et al., 2011] Costa, A. A., Penna, A., and Magenes, G. (2011). Seismic Performance of Autoclaved Aerated Concrete (AAC) Masonry: From Experimental Testing of the In-Plane Capacity of Walls to Building Response Simulation. *Journal of Earthquake Engineering*, 15(1):1–31.

[de Vekey R. C. et al., 1986] de Vekey R. C., Bright, N. J., Luckin, K. R., and Arora, S. K. (1986). The Resistance of Masonry to Lateral Loading . pt. 3. Research results on autoclaved aerated concrete blockwork. *The Structural Engineer*, 64A(11):9.

[Duan et al., 2014] Duan, P., Zhang, Y., Zhou, X., and Miao, Y. (2014). Application of Precast Aerated Concrete Panel Used as External Wallboard in China. *Study of Civil Engineering and Architecture*, 3.

[Kim et al., 2003] Kim, K.-H., Jeon, S.-E., Kim, J.-K., and Yang, S. (2003). An experimental study on thermal conductivity of concrete. *Cement and Concrete Research*, 33(3):363–371.

[MSJC, 2011] MSJC (2011). *Building Code Requirements for Masonry Structures (MSJC).*

[Narayanan and Ramamurthy, 2000] Narayanan, N. and Ramamurthy, K. (2000). Structure and properties of aerated concrete: a review. *Cement and Concrete Composites*, 22(5):321–329.

[Penna et al., 2015] Penna, A., Mandirola, M., Rota, M., and Magenes, G. (2015). Experimental assessment of the in-plane lateral capacity of autoclaved aerated concrete (AAC) masonry walls with flat-truss bed-joint reinforcement. *Construction and Building Materials*, 82:155–166.

[Tanner et al., 2004] Tanner, J., Varela, J., Brightman, M., Cancino, U., Argudo, J., and Klingner, R. (2004). Seismic Performance and Design of Autoclaved Aerated Concrete (AAC) Structural Systems. In *13th World Conference on Earthquake Engineering*, page 14, Vancouver, B.C., Canada.

[Tanner, 2003] Tanner, J. E. (2003). *Design provisions for Autoclaved Aerated Concrete (AAC) structural systems.* PhD thesis, The University of Texas at Austin.

[TEC, 2016] TEC (2016). *Turkish Earthquake Code 2016.*

[TS 12602, 2015] TS 12602 (2015). *FprEN 12602, Prefabricated reinforced components of autoclaved aerated concrete.*

[Varela et al., 2004] Varela, J., Tanner, J., and Klingner, R. (2004). Development of Response Modification Coefficient and Deflection Amplification Factor for Design of AAC Structural Systems. In *13th World Conference on Earthquake Engineering*, page 13, Vancouver, B.C., Canada.

[Varela, 2003] Varela, J. L. (2003). *Development of R and Cd factors for the seismic design of AAC structures.* PhD thesis, The University of Texas at Austin.

[Wilson and Palmer, 2008] Wilson, J. F. and Palmer, W. D. (2008). Designing with autoclaved aerated concrete: New provisions and sustainable properties. *Construction Specifier*, 61(7):40.

[Witfmann and Pytlik, 1992] Witfmann, F. H. and Pytlik, E. C. (1992). Advances in Autoclaved Aerated Concrete Autoclaved Cellular Concrete: The Building Material for The 21st Century. pages 14–16.

[Wittman, 1993] Wittman, F. (1993). *Autoclaved Aerated Concrete-Properties, Testing and Design (RILEM Recommended Practice).* RILEM technical committees.